Selecting the Regularization Parameter in the Distribution of Relaxation Times

Adeleke Maradesa[a], Baptiste Py[a], Ting Hei Wan[a], Mohammed B. Effat[b], Francesco Ciucci[a,c,d*]

[a] Department of Mechanical and Aerospace Engineering, The Hong Kong University of Science and Technology, Hong Kong SAR, China

[b] Department of Mechanical and Power Engineering, Assiut University, Assiut, Egypt

[c] HKUST Shenzhen-Hong Kong Collaborative Innovation Research Institute, Futian, China

[d] Energy Institute, The Hong Kong University of Science and Technology, Hong Kong SAR, China

[*]Corresponding author: francesco.ciucci@ust.hk

Phone: +852 2358 7187

Fax: +852 2358 1543

Abstract

Electrochemical impedance spectroscopy (EIS) is a characterization technique used widely in electrochemistry. Obtaining EIS data is simple when modern electrochemical workstations are used; however, analyzing EIS spectra is still a considerable quandary. The distribution of relaxation times (DRT) has emerged as a solution to this challenge. Nevertheless, DRT deconvolution underlies an ill-posed optimization problem, which is often solved by ridge regression (RR). RR's accuracy strongly depends on the choice of the regularization level as encapsulated in the parameter λ. In this article, five cross-validation methods (*i.e.*, generalized cross-validation, modified generalized cross-validation, robust generalized cross-validation, re-im cross-validation, and k-fold cross-validation) and the L-curve method are studied for the selection of λ. A hierarchical Bayesian DRT (hyper-λ) deconvolution method is also analyzed, whereby λ_0, a parameter analogous to λ, is obtained through cross-validation. The analysis of synthetic data suggests that the values of λ selected by generalized and modified generalized cross-validation are the most accurate among the methods studied. Furthermore, synthetic EIS spectra show that the hyper-λ approach outperforms optimal RR when λ_0 is obtained by generalized and modified generalized cross-validation. This research is expected to foster additional research on the central topic of regularization level selection for DRT analysis. This article not only explores various cross-validation methods, but also provides, through pyDRTtools, an implementation that may serve as a starting point for future research.

Keywords: Electrochemical Impedance Spectroscopy, Distribution of Relaxation Times, Inverse Problem, Cross-Validation, Hyperparametric Methods

1 Introduction

Electrochemical impedance spectroscopy (EIS) is an experimental technique commonly used in electrochemistry [1,2] with broad applications spanning energy science [3], materials [4], medicine [5], and biology [6]. EIS characterization is attractive because it provides frequency-dependent information ranging across several orders of magnitude of timescales (*i.e.*, from mHz to MHz) [7]. Furthermore, modern, state-of-the-art electrochemical workstations afford the collection of high-quality EIS data with limited experimental expertise. Despite these advantages, interpreting EIS spectra remains a considerable challenge [8]. The analysis is usually performed by fitting spectra against equivalent circuits models (ECMs) [9]. However, ECMs are often just circuit analogs and lack uniqueness [10]. Alternatively, physical models can be used, but these models are system-specific and significantly more difficult to implement [6,8,11]. To overcome these challenges, the distribution of relaxation times (DRT) has emerged as a complementary method enabling the identification of the characteristic timescales in EIS spectra [12–17]. Explicitly, within the DRT analysis framework, the impedance model, $Z_{\mathrm{DRT}}(f)$, is fashioned to originate from relaxations, leading to the following expression [10,11,18]:

$$Z_{\mathrm{DRT}}(f) = i2\pi f L_0 + R_\infty + \int_{-\infty}^{\infty} \frac{\gamma(\log \tau)}{1 + i2\pi f\tau} d\log\tau \tag{1}$$

where f, L_0, R_∞, $\gamma(\log\tau)$, and τ are the frequency, inductance, resistance, distribution of relaxation times, and timescale, respectively.

While the DRT model is conceptually simple, deconvolving $\gamma(\log\tau)$ is difficult because the underlying problem is ill-posed [19–23]. Many methodologies have been developed to conduct DRT deconvolution. Those include genetic and evolutionary methods [24,25], Fourier transform methods [15,26], maximum entropy approaches [27], artificial-intelligence-driven methods

[11,28], Gaussian processes [10,18,29], Bayesian and hierarchical Bayesian methods [30–32], and ridge regression (RR) [23,30,33], with RR being arguably the most widely used.

As described in more detail in Section 2.1, in RR, the DRT is obtained by minimizing the sum of squared residuals plus an additional term penalizing "ridges" in $\gamma(\log\tau)$ [14,33]. Namely, if $\boldsymbol{x}$ is (loosely) defined as the vector of the DRT at discrete $\log\tau$ values (a more precise definition and more details are given in Section 2.1.1.1), DRT deconvolution through RR requires solving the following problem [30,33]:

$$\boldsymbol{x} = \underset{\boldsymbol{x}'\geq 0}{\operatorname{argmin}}\left(\left\|\boldsymbol{Z}_{\exp} - \boldsymbol{A}\boldsymbol{x}'\right\|^2 + \lambda\|\boldsymbol{L}\boldsymbol{x}'\|^2\right) \tag{2}$$

where $\|\cdot\|$ is the Euclidean norm, $\boldsymbol{Z}_{\exp}$is a vector of experimental impedances, $\boldsymbol{A}$ is a discretization matrix, and $\lambda\|\boldsymbol{L}\boldsymbol{x}\|^2$ is a penalty. In the latter term, λ is a parameter, and $\boldsymbol{L}$ is a differentiation matrix. The optimal selection of λ is the goal of this article.

The solution to problem (2) strongly depends on λ [30,34], where small and large values of λ result in over-fitting and over-regularization, respectively [35,36]. It is, therefore, imperative to select an appropriate parameter λ when performing RR. In the fields of statistics and inverse problems, several methods have been developed for this purpose, including generalized cross-validation (GCV) [37,38], modified generalized cross-validation (mGCV) [37], robust generalized cross-validation (rGCV) [37], real-imaginary cross-validation (re-im CV) [33,39], *k*-fold generalized cross-validation (kf-CV) [40], and the L-curve (LC) method [41]. Among these methods, only LC [41,42] and re-im CV [14,33] have been used for DRT deconvolution.

Through an array of well-controlled synthetic experiments, this work investigates the quality of the aforementioned methods for the selection of λ in the context of DRT deconvolution and

impedance recovery through RR (Figure 1). For RR, the analysis of synthetic spectra suggests that GCV and mGCV give λ values that are the closest to the optimal ones. It is also shown that λ_0, one of the hyperparameters of the previously developed hierarchical Bayesian method (hyper-λ) (the definition and more details are given in Sections 2.1.1.2 and 2.1.3), can be obtained using GCV and mGCV [31]. Artificial experiments suggest that DRT recovery obtained using hyper-λ methods with λ_0 from CV is generally more accurate than RR, especially for discontinuous and "hook"-type DRTs.

To ensure reproducibility and allow other groups to extend these methods, the software pyDRTtools was updated and shared on GitHub [34]. It is envisioned that this work and the updated pyDRTtools will enable more effective DRT deconvolution and impedance recovery, possibly leading to several follow-up works.

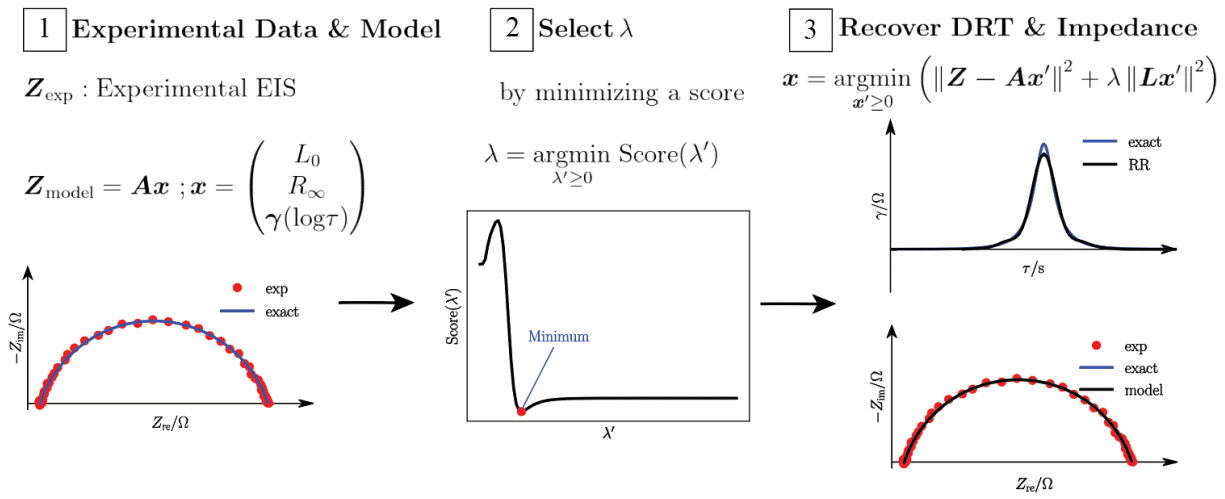

Figure 1. Schematic illustrating the steps taken to select the regularization parameter λ and recover DRT and impedance starting from experimental data.

2 Methods

As already outlined in the Introduction, the outcome of RR strongly depends on λ as defined in (2). As is well known, small values of λ result in noisy DRT (but accurate recovery of the impedance), while large values of λ give smooth DRT (but inaccurate impedance) [34,38]. Therefore, choosing λ "optimally" so as to strike a balance between smoothing the DRT and regressing the impedance is key to DRT deconvolution. This section first outlines the DRT deconvolution nomenclature, then it illustrates how to obtain an "optimal" λ using an array of statistics-oriented methods.

2.1 Theory

2.1.1 DRT Deconvolution

2.1.1.1 Ridge Regression

We start by introducing the quantities and corresponding notations used thereafter. Following our previous articles [33,34], the real and imaginary parts of the DRT impedance model vector given by $\boldsymbol{Z}_{\mathrm{DRT}} = \boldsymbol{Z}_{\mathrm{DRT,re}} + i\boldsymbol{Z}_{\mathrm{DRT,im}}$ are approximated as follows:

$$\boldsymbol{Z}_{\mathrm{DRT,re}} = R_{\infty}\mathbf{1} + \boldsymbol{A}_{\gamma,\mathrm{re}}\boldsymbol{\gamma} \tag{3a}$$

$$\boldsymbol{Z}_{\mathrm{DRT,im}} = 2\pi L_0\boldsymbol{f} + \boldsymbol{A}_{\gamma,\mathrm{im}}\boldsymbol{\gamma} \tag{3b}$$

with $(\boldsymbol{\gamma})_n = \gamma(\log\tau_n)$ for $n = 1,\ 2,\ldots,\ N$, and $\left(\boldsymbol{Z}_{\mathrm{DRT,re}}\right)_m = \mathrm{Re}\left(Z_{\mathrm{DRT}}(f_m)\right)$, $\left(\boldsymbol{Z}_{\mathrm{DRT,im}}\right)_m = \mathrm{Im}\left(Z_{\mathrm{DRT}}(f_m)\right)$, $\mathbf{1}$ is an N-dimentional column vector of ones, and $(\boldsymbol{f})_m = f_m$ for $m = 1, 2, \ldots, M$. The $\log\tau_n$ values are the log timescales at which $\gamma(\log\tau)$ is approximated, and the f_m values are the experimental frequencies. $\boldsymbol{A}_{\gamma,\mathrm{re}}$ and $\boldsymbol{A}_{\gamma,\mathrm{im}}$ are discretization matrices given elsewhere [34].

The following two matrices can also be defined:

$$\boldsymbol{A}_{\mathrm{re}} = \left(\mathbf{0} \mid \mathbf{1} \mid \boldsymbol{A}_{\gamma,\mathrm{re}}\right) \tag{4a}$$

$$\boldsymbol{A}_{\mathrm{im}} = \left(2\pi\boldsymbol{f} \mid \mathbf{0} \mid \boldsymbol{A}_{\gamma,\mathrm{im}}\right) \tag{4b}$$

where $\mathbf{0}$ is an M-dimensional column vector of zeros. In turn, the matrix $\boldsymbol{A}$ in (2) can be defined as

$$\boldsymbol{A} = \begin{pmatrix}\boldsymbol{A}_{\mathrm{re}}\\ \boldsymbol{A}_{\mathrm{im}}\end{pmatrix} \tag{5}$$

Then, $\boldsymbol{x} = (R_\infty, L_0, \boldsymbol{\gamma}^\top)^\top$ can be estimated by solving (2) where $\boldsymbol{Z}_{\text{exp}} = \begin{pmatrix} \boldsymbol{Z}_{\text{exp,re}} \\ \boldsymbol{Z}_{\text{exp,im}} \end{pmatrix}$ with $\boldsymbol{Z}_{\text{exp,re}}$ and $\boldsymbol{Z}_{\text{exp,im}}$ being the vectors of real and imaginary parts of the experimental impedance, respectively.

2.1.1.2 Hyper-$\boldsymbol{\lambda}$ Ridge Regression

In a hierarchical Bayesian framework, λ is a $\log \tau$-dependent random variable [30,31]. Thus, the implementation needs a random vector $\boldsymbol{\lambda} \in \mathbb{R}^{N_\lambda}$ with N_λ defined as $N_\lambda = M - q$ where M is the number of EIS frequencies and q is the derivative order of the differentiation matrix $\boldsymbol{L}$ in (2) [30]. As explained in earlier publications [30,31], the probability, $p(\boldsymbol{x}, \boldsymbol{\lambda} | \boldsymbol{Z}_{\text{exp}})$, of $\boldsymbol{x}$ and $\boldsymbol{\lambda}$ given the experimental impedance $\boldsymbol{Z}_{\text{exp}}$ is given by

$$p(\boldsymbol{x}, \boldsymbol{\lambda} | \boldsymbol{Z}_{\text{exp}}) p(\boldsymbol{Z}_{\text{exp}}) = p(\boldsymbol{x}, \boldsymbol{\lambda}) p(\boldsymbol{Z}_{\text{exp}} | \boldsymbol{x}, \boldsymbol{\lambda}) \tag{6}$$

where $p(\boldsymbol{Z}_{\text{exp}})$ is the probability of observing the specific experimental EIS vector $\boldsymbol{Z}_{\text{exp}}$ (this results in a constant), and $p(\boldsymbol{Z}_{\text{exp}} | \boldsymbol{x}, \boldsymbol{\lambda})$ is the likelihood of the experimental data given $\boldsymbol{x}$. The prior on $\boldsymbol{x}$ and $\boldsymbol{\lambda}$ jointly, $p(\boldsymbol{x}, \boldsymbol{\lambda})$, can be rewritten as

$$p(\boldsymbol{x}, \boldsymbol{\lambda}) = p(\boldsymbol{x} | \boldsymbol{\lambda}) p(\boldsymbol{\lambda}) \tag{7}$$

By choosing a Gaussian prior on $\boldsymbol{x}$, *i.e.*, $\boldsymbol{L}\boldsymbol{x} \sim \mathcal{N}(0, \boldsymbol{\Lambda}^{-1})$ with $(\boldsymbol{\Lambda})_{hk} = \begin{cases} 0 \ \ if \ h \neq k \\ (\boldsymbol{\lambda})_k \ \ if \ h = k \end{cases}$ for $h, k = 1, 2, \ldots, N_\lambda$, the prior $p(\boldsymbol{x} | \boldsymbol{\lambda})$ can be rewritten as

$$p(\boldsymbol{x} | \boldsymbol{\lambda}) \propto \mathbf{1}(\boldsymbol{x} \geq 0) \prod_{k=1}^{N_\lambda} \sqrt{\frac{(\boldsymbol{\lambda})_k}{2\pi}} \exp\left(-\frac{(\boldsymbol{\lambda})_k}{2} (\boldsymbol{L}\boldsymbol{x})_k^2 \right) \tag{8}$$

In this work, we set $q = 2$; in other words, $\boldsymbol{L}$ is used to approximate $\frac{d^2\gamma(\log\tau)}{d\log\tau^2}$. The indicator function $\mathbf{1}(\boldsymbol{x} \geq 0)$ (equal to 1 if all entries in $\boldsymbol{x}$ are positive, and 0 otherwise) is used to enforce the non-negativity constraint on the DRT.

All components of $\boldsymbol{\lambda}$ are taken to be independent and identically distributed with the following Gamma hyperprior distribution:

$$p_{\mathrm{HP}}((\boldsymbol{\lambda})_k, \boldsymbol{\xi}) = (\boldsymbol{\lambda})_k^{\frac{\beta}{2}-1} \exp\left(-\frac{\beta-1}{2\lambda_0}(\boldsymbol{\lambda})_k\right) \tag{9}$$

with the parameter vector defined as $\boldsymbol{\xi} = \begin{pmatrix}\beta \\ \lambda_0\end{pmatrix}$, where β is the parameter of the hyperprior distribution, and λ_0 is the nominal regularization level[1].

The prior $p(\boldsymbol{\lambda})$ in (7) is then given by [30,31]

$$p(\boldsymbol{\lambda}) = \prod_{j=1}^{N_\lambda} \mathbf{1}((\boldsymbol{\lambda})_k \geq 0) p_{\mathrm{HP}}((\boldsymbol{\lambda})_k, \boldsymbol{\xi}) \tag{10}$$

We note that the maximum a posteriori (MAP) estimate of $\boldsymbol{x}$ and $\boldsymbol{\lambda}$ are obtained by alternate minimization, as described in [31], and the $(\boldsymbol{\lambda})_k$ values are given analytically by [30,31]

$$(\boldsymbol{\lambda})_k = \frac{\lambda_0}{\frac{\lambda_0}{\beta-1}(\boldsymbol{L}\boldsymbol{x})_k^2 + 1} \tag{11}$$

2.1.2 Hyperparameter Selection with the CV and LC Scores

As shown in the central panel of Figure 1, λ is determined by minimizing a score function. The seven scores used in this work are described in the present section.

[1] We note that λ_0, from (11), is the regularization level obtained for $\boldsymbol{L}\boldsymbol{x} = \mathbf{0}$.

2.1.2.1 Optimal λ

The optimal λ, λ_{opt}, is obtained by solving the following problem:

$$\lambda_{\text{opt}} = \underset{\lambda \geq 0}{\operatorname{argmin}} \left\| \boldsymbol{\gamma}_{\text{exact}}(\log \boldsymbol{\tau}) - \boldsymbol{\gamma}(\lambda) \right\|^2 \tag{12}$$

Where $\left(\boldsymbol{\gamma}_{\text{exact}}(\log \boldsymbol{\tau})\right)_n = \gamma_{\text{exact}}(\log \tau_n)$ for $n = 1, 2, \ldots, N$ [2], and $\boldsymbol{\gamma}(\lambda)$ is the DRT part of the $\boldsymbol{x}$ vector obtained by solving (2)[3].

2.1.2.2 Cross-Validation Methods

CV is a statistical method utilized for model selection, performance estimation, and learning/tuning model parameters [43]. Only the re-im CV method proposed by Saccoccio *et al.* [33] has been used for DRT parameter selection. Other CV methods have yet to be used for DRT parameter selection. In this section, GCV, mGCV, rGCV, kf, and re-im CV are overviewed and applied to DRT deconvolution.

2.1.2.2.1 Generalized Cross-Validation

GCV has been used, in statistics and machine learning, for computing the regularization parameters [38]. Following the seminal work of Wahba *et al.*, GCV determines λ by minimizing the following function [38]:

$$\text{GCV}(\lambda) = \frac{(2M)^{-1} \left\| \left(\boldsymbol{I} - \boldsymbol{K}(\lambda)\right) \boldsymbol{Z}_{\text{exp}} \right\|^2}{\left[(2M)^{-1} \text{tr}\left(\boldsymbol{I} - \boldsymbol{K}(\lambda)\right)\right]^2} \tag{13}$$

[2] $\boldsymbol{\gamma}_{\text{exact}}$ was selected to be the analytical DRT (Table S1 of the supplementary information (SI)) for synthetic experiments. For real EIS data, we used the DRT obtained from the regressed ECM, which is denoted as $\boldsymbol{\gamma}_{\text{ECM}}$ (see Section 3.2).

[3] λ_{opt} depends on the $\log \boldsymbol{\tau}$ chosen.

$\boldsymbol{K}(\lambda) = \mathbf{A}(\mathbf{A}^\top\mathbf{A} + \lambda\boldsymbol{L}^\top\boldsymbol{L})^{-1}\mathbf{A}^\top \in \mathbb{R}^{2M\times 2M}$ and $\boldsymbol{I}$ is the $2M \times 2M$ identity matrix. The reader is invited to consult Section S1.1 for the derivation.

2.1.2.2.2 Modified Generalized Cross-Validation

To stabilize the GCV, Kim *et al*. [44] developed the mGCV criterion, which minimizes the following function:

$$\mathrm{mGCV}(\lambda) = \frac{(2M)^{-1}\left\|\left(\boldsymbol{I} - \boldsymbol{K}(\lambda)\right)\boldsymbol{Z}_{\exp}\right\|^2}{\left[(2M)^{-1}\mathrm{tr}\left(\boldsymbol{I} - \rho\boldsymbol{K}(\lambda)\right)\right]^2} \tag{14}$$

where $\rho > 1$ is a stabilization parameter calculated using the following empirical rule:

$$\rho = \begin{cases} 1.3 \text{ if } M < 50 \\ 2 \text{ if } M \geq 50 \end{cases} \tag{15}$$

2.1.2.2.3 Robust Generalized Cross-Validation

The rGCV method can be used to overcome under-smoothing arising when the sample size is too small. To that end, the rGCV method minimizes a weighted average of the GCV given by [35,37]

$$\mathrm{rGCV}(\lambda) = \left(\xi + (1-\xi)\mu_2(\lambda)\right)\mathrm{GCV}(\lambda) \tag{16}$$

Where $\mu_2(\lambda) = (2M)^{-1}\mathrm{tr}\left(\boldsymbol{K}^2(\lambda)\right)$ and the rule $\xi = \begin{cases} 0.2 \text{ if } M < 50 \\ 0.3 \text{ if } M \geq 50 \end{cases}$ was used to calculate the robust parameter ξ [37].

2.1.2.2.4 Re-Im Cross-Validation

In re-im CV, the real, $\boldsymbol{Z}_{\exp,\mathrm{re}}$, and imaginary, $\boldsymbol{Z}_{\exp,\mathrm{im}}$, parts of the experimental impedance vector defined in Section 2.1.1.1 can be used separately to determine two values of $\boldsymbol{x}$, called $\boldsymbol{x}_{\mathrm{re}}$ and $\boldsymbol{x}_{\mathrm{im}}$, respectively [33]. In the re-im CV approach, the following sum of squared errors of $\boldsymbol{Z}_{\exp,\mathrm{re}}$ and $\boldsymbol{Z}_{\exp,\mathrm{im}}$ is minimized:

$$\text{re-im}(\lambda) = \left\|\boldsymbol{Z}_{\text{exp,re}} - \boldsymbol{A}_{\text{re}}\boldsymbol{x}_{\text{re}}\right\|^2 + \left\|\boldsymbol{Z}_{\text{exp,im}} - \boldsymbol{A}_{\text{im}}\boldsymbol{x}_{\text{im}}\right\|^2 \tag{17}$$

2.1.2.2.5 k-Fold Cross-Validation

In kf-CV, the experimental impedance, $\boldsymbol{Z}_{\text{exp}}$, is initially partitioned into k subsamples or "folds" of equal size. The p-th partition ($p = 1, 2, \ldots, k$) $\boldsymbol{Z}_{p,\text{test}}$ is treated as the test set, while the rest of $\boldsymbol{Z}_{\text{exp}}$ is used to estimate the DRT vector, $\boldsymbol{x}_p(\lambda)$, by solving an optimization problem formally equivalent to (2). Then, using $\boldsymbol{x}_p(\lambda)$ and $\boldsymbol{Z}_{p,\text{test}}$, the square residuals between predicted and test impedance are computed (see (S9) in Section S1.2). Finally, the kf-CV score, $\text{kf}(\lambda)$, is obtained as the average of these residuals [40]. We emphasize that, as k increases, so does the computational time. In this article, we chose $k = 5$ [45].

2.1.2.3 L-Curve

In the L-curve approach, the optimal λ maximizes the curvature of the function defined as the logarithm of the squared residual, $\eta(\lambda) = \log\left(\|\boldsymbol{Z}_{\text{exp}} - \boldsymbol{A}\boldsymbol{x}(\lambda)\|^2\right)$, versus the logarithm of the regularization penalty, $\theta(\lambda) = \log(\lambda\|\boldsymbol{L}\boldsymbol{x}(\lambda)\|^2)$ [41], where $\boldsymbol{x}(\lambda)$ is computed by solving (2). In short,

$$\lambda_{\text{LC}} = \underset{\lambda \geq 0}{\text{argmax}}\, \text{LC}(\lambda) \tag{18}$$

where

$$\text{LC}(\lambda) = \frac{\frac{d^2\theta(\lambda)}{d\lambda^2}\frac{d\eta(\lambda)}{d\lambda} - \frac{d\theta(\lambda)}{d\lambda}\frac{d^2\eta(\lambda)}{d\lambda^2}}{\left(\left(\frac{d\theta(\lambda)}{d\lambda}\right)^2 + \left(\frac{d\eta(\lambda)}{d\lambda}\right)^2\right)^{3/2}} \tag{19}$$

2.1.3 CV-based Selection of the DRT Regularization Parameter in Hyper-λ

In the hyper-λ framework (Section 2.1.1.2), the regularization vector $\boldsymbol{\lambda}$ is a function of the two-dimensional vector $\boldsymbol{\xi} = \begin{pmatrix} \beta \\ \lambda_0 \end{pmatrix}$, see (11). While the tunable parameters β and λ_0 provide the hyper-λ method with more flexibility over RR, herein, we set β = 2 so that the hyperprior $p_{\mathrm{HP}}(\lambda, \boldsymbol{\xi})$ in (9) becomes an exponential distribution [30,46]. The λ_0 was selected using GCV and mGCV. The optimal λ_0, indicated as $\lambda_{0,\mathrm{opt}}$, was computed by solving a problem analogous to (12) in Section 2.1.2.1[4].

2.2 Implementation

We generated artificial experiments in the $10^{-2} - 10^{6}$ Hz frequency range with 10 points per decade [47,48]. For the exact impedance $Z_{\mathrm{exact}}(f)$, we studied the single ZARC, 2×ZARC, piecewise constant (PWC), Gerischer, and "hook" models [30,49]. Table S1 shows the analytical expressions of each impedance and DRT model; the parameters used are reported in Tables S2, S3, and S4. Each synthetic impedance $Z_{\mathrm{exp}}(f)$ was obtained by corrupting the exact impedance with various error models.

As a first step, uniform errors were considered:

$$Z_{\mathrm{exp}}(f) = Z_{\mathrm{exact}}(f) + \sigma_n^{\mathrm{exp}}(\varepsilon_{\mathrm{re}} + i\varepsilon_{\mathrm{im}}) \tag{20}$$

where the real, $\varepsilon_{\mathrm{re}}$, and imaginary, $\varepsilon_{\mathrm{im}}$, components of the error are independent and identically distributed with $\varepsilon_{\mathrm{re}}$, $\varepsilon_{\mathrm{im}} \sim \mathcal{N}(0,1)$. Unless otherwise specified, the error level σ_n^{exp} was set to 0.2 Ω.

[4] $\lambda_{0,\mathrm{opt}}$ was obtained as $\lambda_{0,\mathrm{opt}} = \underset{\lambda_0 \geq 0}{\mathrm{argmin}} \left\| \boldsymbol{\gamma}_{\mathrm{exact}}(\log \boldsymbol{\tau}) - \boldsymbol{\gamma}_{\mathrm{hyper}}(\beta = 2, \lambda_0) \right\|^2$ where $\gamma_{\mathrm{hyper}}(\beta = 2, \lambda_0)$ is obtained from MAP.

Two frequency-dependent error models were also considered, namely,

$$Z_{\text{exp}}(f) = Z_{\text{exact}}(f) + \xi_n^{\text{exp}} |Z_{\text{exact}}(f)| (\varepsilon_{\text{re}} + i\varepsilon_{\text{im}}) \tag{21a}$$

$$Z_{\text{exp}}(f) = Z_{\text{exact}}(f) + \xi_n^{\text{exp}} \left(\left| Z_{\text{exact,re}}(f) \right| \varepsilon_{\text{re}} + i \left| Z_{\text{exact,im}}(f) \right| \varepsilon_{\text{im}} \right) \tag{21b}$$

where ξ_n^{exp} is a scalar, whose value will be given in the corresponding section (Section 3.1.1.4). For RR deconvolution, λ (given $Z_{\text{exp}}(f)$) was selected using all parameter selection methods described in Section 2.1.2 in the range from 10^{-7} to 10^{-1} by minimizing the corresponding score (Section 2.1.2.2). The vector $\boldsymbol{x}$ was obtained by solving (2) using the λ values obtained using each model. For the hyper-λ methods, $\boldsymbol{x}$ was obtained through the alternate minimization algorithm described in Section 2.1.1.2. We must stress that the non-negativity constraint in (2) was not enforced for "hook" EIS spectra (Section 3.1.4). For all the methods, the DRT impedance, $\boldsymbol{Z}_{\text{DRT}}$, was computed using $\boldsymbol{Z}_{\text{DRT}} = \boldsymbol{A}\boldsymbol{x}$.

2.3 Quality Scores

To compare the values of λ obtained from each parameter selection method to λ_{opt} in (12), the absolute error on λ, abs_λ, the normalized absolute error on λ, $\text{abs}_{\text{norm},\lambda}$, and the mean squared error on λ, MSE_λ, were introduced:

$$\text{abs}_\lambda = \frac{1}{N_{\text{exp}}} \sum_{k=1}^{N_{\text{exp}}} \left| \lambda_{\text{opt},k} - \lambda_{\text{CV},k} \right| \tag{22a}$$

$$\text{abs}_{\text{norm},\lambda} = \frac{1}{N_{\text{exp}}} \sum_{k=1}^{N_{\text{exp}}} \frac{\left| \lambda_{\text{opt},k} - \lambda_{\text{CV},k} \right|}{\bar{\lambda}_{\text{opt}}} \tag{22b}$$

$$\mathrm{MSE}_{\lambda} = \frac{1}{N_{\mathrm{exp}}} \sum_{k=1}^{N_{\mathrm{exp}}} \left(\lambda_{\mathrm{opt},k} - \lambda_{\mathrm{CV},k}\right)^2 \tag{22c}$$

where N_{exp} is the number of synthetic experiments, λ_{opt} is the optimal λ (Section 2.1.2.1) whose average $\bar{\lambda}_{\mathrm{opt}}$ is $\bar{\lambda}_{\mathrm{opt}} = \frac{1}{N_{\mathrm{exp}}} \sum_{k=1}^{N_{\mathrm{exp}}} \lambda_{\mathrm{opt},k}$, and λ_{CV} is the λ selected using a given parameter regularization method.

To score the accuracy of DRT recovery, the normalized DRT square error, $\mathrm{SE}_{\mathrm{norm},\gamma}$, and the normalized DRT mean square error, $\mathrm{MSE}_{\mathrm{norm},\gamma}$, were used:

$$\mathrm{SE}_{\mathrm{norm},\gamma} = \frac{\|\boldsymbol{\gamma}_{\mathrm{exact}} - \boldsymbol{\gamma}_{\mathrm{CV}}(\lambda)\|^2}{\|\boldsymbol{\gamma}_{\mathrm{exact}}\|^2} \tag{23a}$$

$$\mathrm{MSE}_{\mathrm{norm},\gamma} = \frac{1}{N_{\mathrm{exp}}} \sum_{k=1}^{N_{\mathrm{exp}}} \frac{\left\|\boldsymbol{\gamma}_{\mathrm{exact}} - \boldsymbol{\gamma}_{\mathrm{CV},k}(\lambda)\right\|^2}{\|\boldsymbol{\gamma}_{\mathrm{exact}}\|^2} \tag{23b}$$

where $\boldsymbol{\gamma}_{\mathrm{exact}}$ is the exact DRT, and $\boldsymbol{\gamma}_{\mathrm{CV}}(\lambda)$ is the DRT recovered with a given parameter regularization method.

Lastly, we introduce the normalized impedance mean square error, $\mathrm{MSE}_{\mathrm{norm},z}$, as

$$\mathrm{MSE}_{\mathrm{norm},z} = \frac{1}{N_{\mathrm{exp}}} \sum_{k=1}^{N_{\mathrm{exp}}} \frac{\left\|\boldsymbol{Z}_{\mathrm{exact}} - \boldsymbol{Z}_{\mathrm{CV},k}(\lambda)\right\|^2}{\|\boldsymbol{Z}_{\mathrm{exact}}\|^2} \tag{24}$$

where $\boldsymbol{Z}_{\mathrm{exact}}$ is the exact impedance, and $\boldsymbol{Z}_{\mathrm{CV}}(\lambda)$ the impedance recovered with a given parameter regularization method.

3 Results

Synthetic experiments were used to investigate the accuracy of the different λ-selection scores. Then, the two best scores were used to select the hyperparameter λ_0 (for the hyper-λ methods) optimally. Finally, the accuracy of these two hyper-λ methods was investigated with synthetic and real EIS data from three batteries and one fuel cell.

3.1 Artificial Experiments

3.1.1 Single ZARC Model

3.1.1.1 Investigation of the Optimal Method

First, we studied a single ZARC model. Panels (a), (c), and (e) of Figure 2 show the experimental, exact, and recovered impedances for one synthetic experiment using the optimal, GCV, and mGCV scores, respectively. The corresponding DRTs are presented in panels (b), (d), and (f) of Figure 2. The DRT and impedance recoveries appear close to the exact ones for all three methods except for slight DRT oscillations at $\tau \approx 10^{-3}$ s and 10^{-1} s.

Next, 500 artificial experiments were generated. Figure 3 (a) shows the boxplot of the λ values of all optimized scores. It is worth stressing that the notch, rhombus, and whiskers refer to the median, 25-75% interquartile range, and 1.5 times this range, respectively. LC, mGCV, and rGCV methods have the highest λ values[5] (Figure 3 (a)), which leads to over-smoothing (panels (f) and (h) of Figure S1 and Figure S2 (b), respectively). Conversely, optimizing the GCV, re-im CV, and kf-CV scores allowed the identification of the DRT peak, and led to better DRT recoveries (Figure S1 (d) and panels (d) and (f) of Figure S2, respectively). For all methods, the impedance of the

[5] Note that the values of λ selected by the optimal, a given CV, and the LC method are denoted as λ_{opt}, λ_{CV}, and λ_{LC}, respectively.

single ZARC model was recovered well (left panel of Figures S1 and S2). As expected from (12), the optimal λ_{opt} leads to the lowest normalized square errors, $\mathrm{SE}_{\mathrm{norm},\gamma}$, as shown in Figure 3 (b).

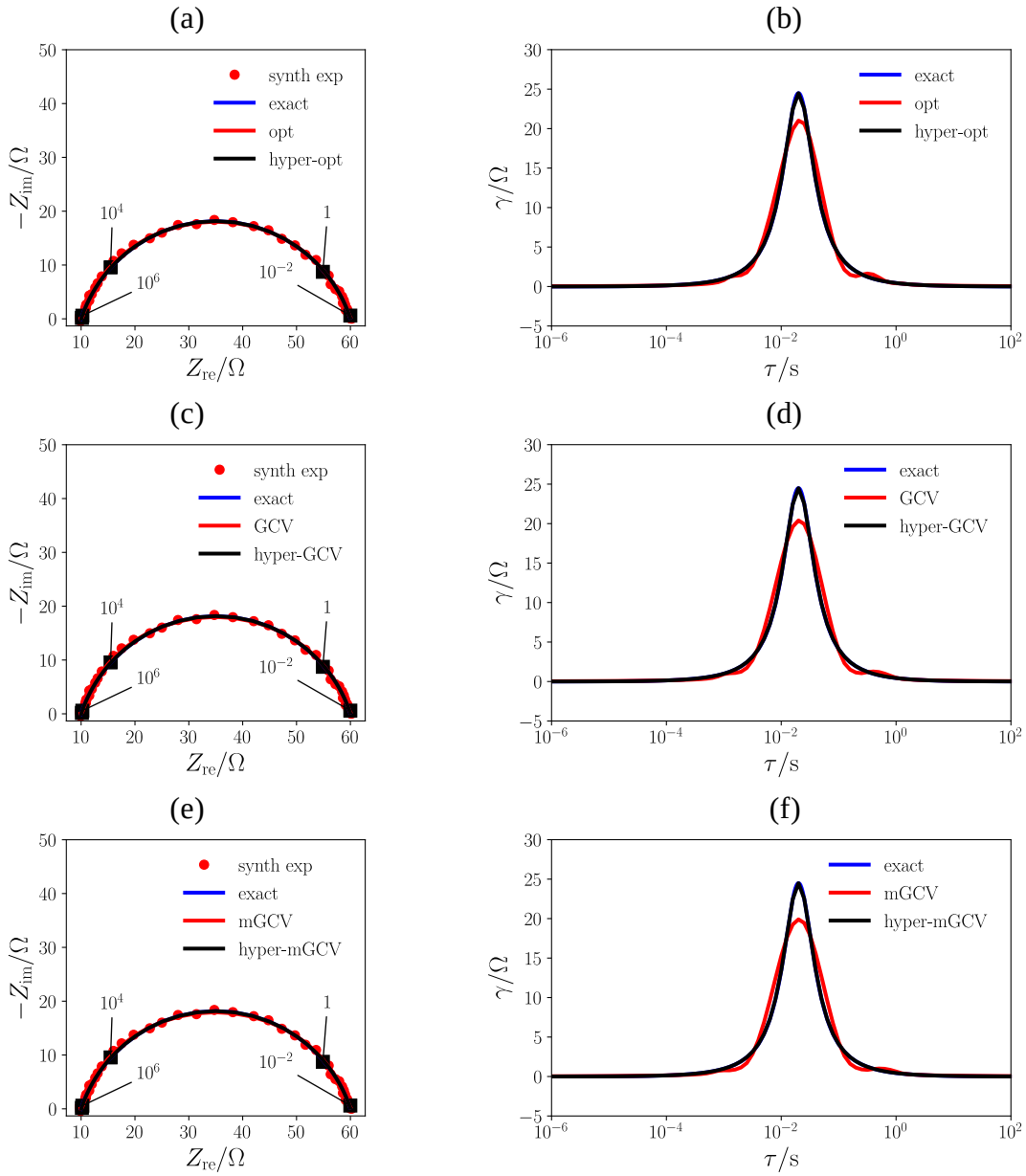

Figure 2. For the single ZARC model ($\sigma_n^{\mathrm{exp}} = 0.2\,\Omega$), exact, experimental, and recovered impedances based on (a) optimal and hyper-optimal, (c) GCV and hyper-GCV, and (e) mGCV and hyper-mGCV methods are shown. Exact and recovered DRTs are shown in panels (b), (d), and (f).

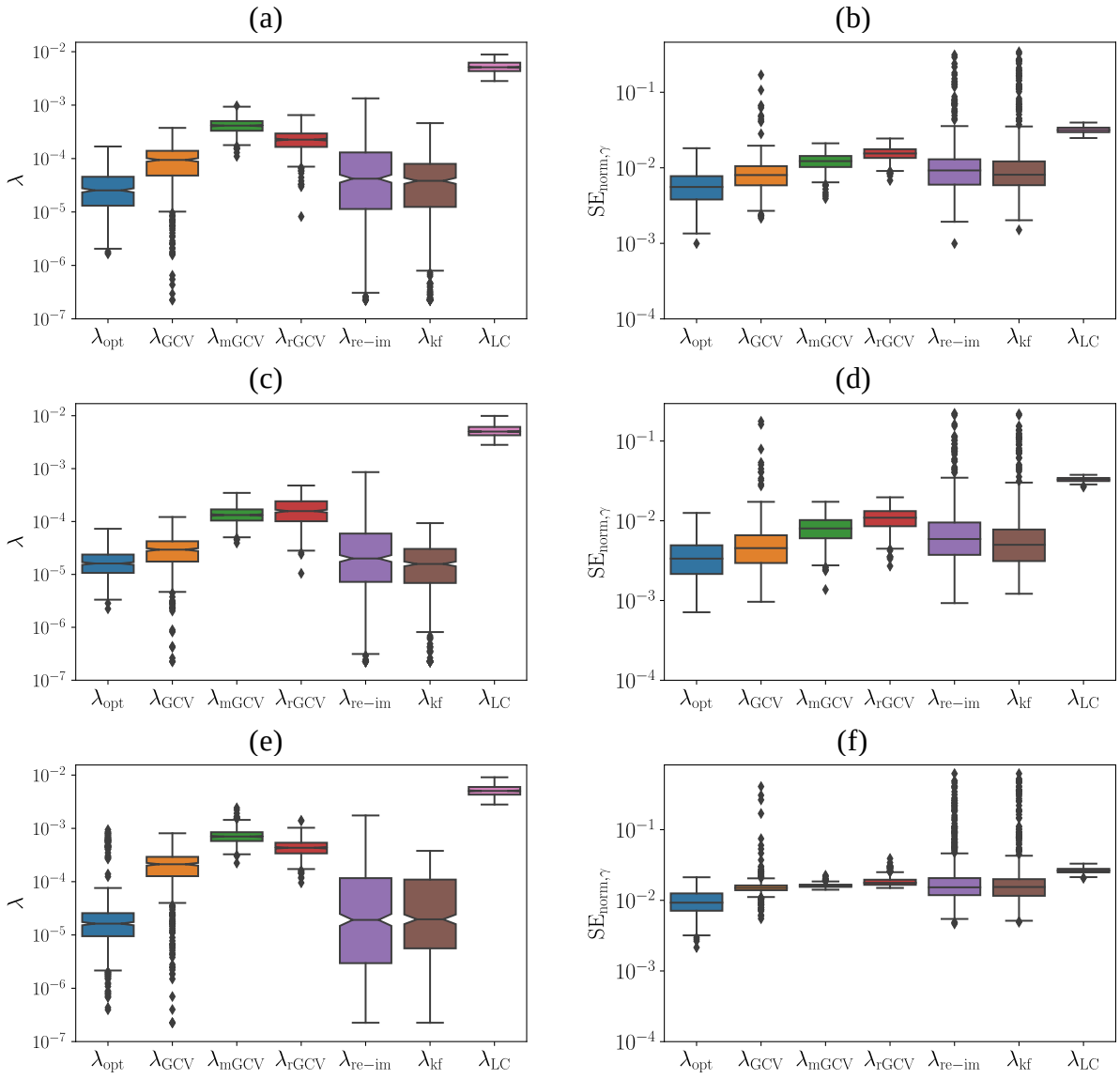

Figure 3. Boxplots of the optimal λ values shown together with the ones minimizing each score ($\sigma_n^{\exp} = 0.2\ \Omega$). The λ shown were obtained using 500 synthetic experiments and the (a) single ZARC, (c) overlapping 2×ZARC, and (e) PWC models. Corresponding boxplots of $\mathrm{SE}_{\mathrm{norm},\gamma}$ are reported in panels (b), (d), and (f).

3.1.1.2 Correlation between λ and λ_{opt}

To show the joint distribution between the optimal λ_{opt} and the λ values selected using each parameter regularization method, we plot in Figure 4 the correlation plots with their respective

marginal distributions. We observe that λ_{LC}, λ_{mGCV}, and λ_{rGCV} are strongly correlated with λ_{opt}. Interestingly, the values of λ_{mGCV}, and λ_{rGCV} are densely concentrated around $\lambda_{\mathrm{mGCV}} = \lambda_{\mathrm{rGCV}} \approx 10^{-4}$, while the LC values are mostly concentrated around $\lambda_{\mathrm{LC}} \approx 10^{-3}$, see panels (b), (c), and (f) of Figure 4. These high λ values explain the under-recovered DRTs when the λ used is obtained via these methods (panels (f) and (h) of Figure S1 and Figure S2 (b)). Conversely, the λ_{CV} values from GCV, re-im CV, and kf-CV are visually closer to λ_{opt} as shown by a distribution centered near the diagonal, which explains the more accurate identification of the DRT peak in Figure S1 (d) and in panels (d) and (f) of Figure S2, respectively.

To assess how λ_{LC}, λ_{mGCV}, and λ_{rGCV} correlate with λ_{opt}, the scores introduced in Section 2.3 were used. GCV presents the lowest values for all the scores, with kf-CV coming second, see Table 1 and Table S5. The wall clock time needed to minimize each score was also computed (Table 1). The GCV and kf-CV were the fastest and slowest methods, respectively.

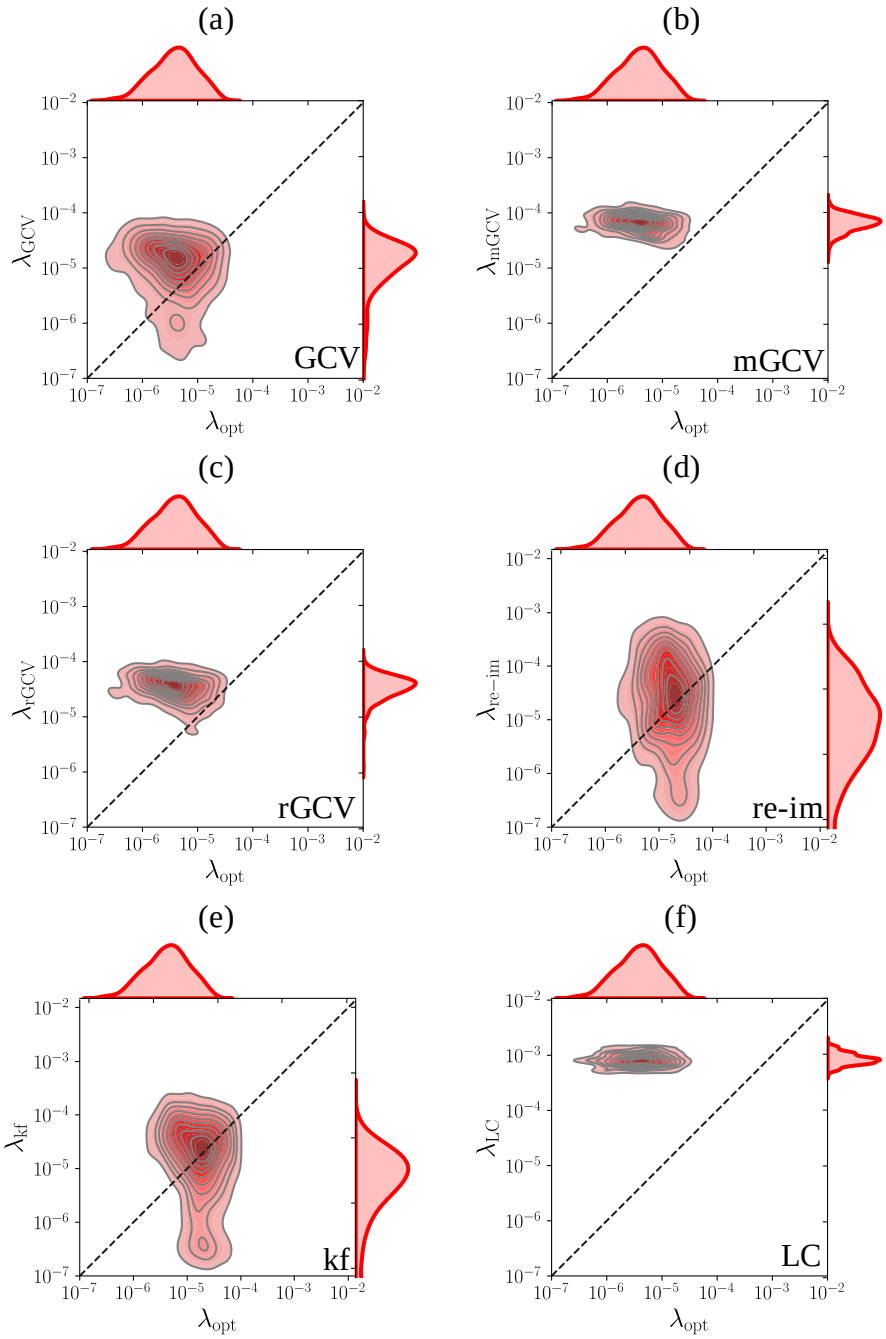

Figure 4. For the single ZARC model ($\sigma_n^{\mathrm{exp}} = 0.2\ \Omega$), correlation plot between the optimal λ_{opt} and (a) λ_{GCV}, (b) λ_{mGCV}, (c) λ_{rGCV}, (d) $\lambda_{\mathrm{re-im}}$, (e) λ_{kf}, and (f) λ_{LC} as obtained using 500 synthetic experiments.

Table 1. For the single ZARC model ($\sigma_n^{\exp} = 0.2\ \Omega$ and 500 synthetic experiments), abs_{λ}, $\mathrm{abs}_{\mathrm{norm},\lambda}$, MSE_{λ}, $\mathrm{MSE}_{\mathrm{norm},Z_{\mathrm{opt}}}$, $\mathrm{MSE}_{\mathrm{norm},Z_{\mathrm{exp}}}$, $\mathrm{MSE}_{\mathrm{norm},Z_{\mathrm{exact}}}$, $\mathrm{MSE}_{\mathrm{norm},\gamma_{\mathrm{opt}}}$, $\mathrm{MSE}_{\mathrm{norm},\gamma_{\mathrm{exact}}}$[6], and clock time for each parameter regularization method.

Method	abs_{λ}	$\mathrm{abs}_{\mathrm{norm},\lambda}$	MSE_{λ}	$\mathrm{MSE}_{\mathrm{norm},Z_{\mathrm{opt}}}$	$\mathrm{MSE}_{\mathrm{norm},Z_{\mathrm{exp}}}$	$\mathrm{MSE}_{\mathrm{norm},Z_{\mathrm{exact}}}$	$\mathrm{MSE}_{\mathrm{norm},\gamma_{\mathrm{opt}}}$	$\mathrm{MSE}_{\mathrm{norm},\gamma_{\mathrm{exact}}}$	Clock time (s)
GCV	**6.060E-5**	**8.213E-5**	**6.353E-9**	**4.621E-9**	**5.661E-5**	**2.883E-7**	**1.236E-5**	**1.143E-3**	**8.839E-2±3.618E-2**
mGCV	3.372E-4	3.643E-4	1.318E-7	1.597E-6	6.032E-5	2.672E-6	7.867E-3	2.075E-2	8.049E-1±2.537E-1
rGCV	6.820E-4	7.275E-4	5.149E-7	3.609E-6	6.263E-5	4.980E-6	1.426E-5	2.608E-2	9.995E-1±4.563E-1
re-im CV	9.720E-5	3.619E-4	3.763E-8	6.382E-6	5.802E-5	4.867E-7	1.689E-5	1.509E-2	4.619E0±2.145E0
kf-CV	8.822E-5	8.229E-5	1.187E-7	8.460E-8	5.876E-5	5.612E-7	5.624E-4	8.734E-3	8.175E0±4.730E0
LC	5.641E-3	5.960E-3	3.433E-5	2.917E-5	8.905E-5	3.157E-5	3.431E-2	4.944E-2	1.664E0±1.036E0

[6] The mean square errors with respect to $\boldsymbol{\gamma}_{\mathrm{opt}}$ and $\boldsymbol{\gamma}_{\mathrm{exact}}$ are defined as $\mathrm{MSE}_{\mathrm{norm},\gamma_{\mathrm{opt}}}$ and $\mathrm{MSE}_{\gamma_{\mathrm{exact}}}$, respectively. Similarly, we define the normalized mean square impedance error on the impedance recovered using Z_{opt}, Z_{exp}, and Z_{exact} as $\mathrm{MSE}_{Z_{\mathrm{opt}}}$, $\mathrm{MSE}_{Z_{\mathrm{exp}}}$, and $\mathrm{MSE}_{Z_{\mathrm{exact}}}$, respectively.

3.1.1.3 Influence of the Experimental Error on the Regularization Parameter Values

The influence of $\sigma_n^{\exp}$, the experimental noise level, on the λ from CV and LC methods was also studied. Specifically, we repeated the same procedure described in Section 3.1.1.1 with $\sigma_n^{\exp} = 0.4, 0.6, 0.8,$ and $1.0\,\Omega$. Graphically, Figures S3–S4, S5–S6, S7–S8, and S9–S10 show the averaged recovered impedances and DRTs using each parameter regularization method for $\sigma_n^{\exp} =$ 0.4, 0.6, 0.8, and 1.0 Ω, respectively. For increasing $\sigma_n^{\exp}$, we note that the impedance recovery with the GCV, mGCV, re-im CV, and kf-CV methods are more accurate compared to the rGCV and LC methods. Quantitatively, the values of all the scores reported in Table S5 increase with $\sigma_n^{\exp}$, indicating an increasing distance between the optimal λ_{opt} and the selected λ as $\sigma_n^{\exp}$ increases. Moreover, consistent with the experiments of Section 3.1.1.1, GCV and mGCV remain the most accurate methods for this set of experiments (Table S5).

3.1.1.4 Frequency-Dependent Error Models

In this section, the two frequency-dependent error models are studied for $\xi_n^{\exp} = 0.02$ (Section 2.2). Figures S11 and S12 show the averaged recovered impedances and DRTs using each parameter regularization method for the error model in (21a). The LC and rGCV methods slightly under-recovered the exact DRT (Figure S11 (f) and Figure S12 (b), respectively), and the corresponding recovered impedances slightly mismatched the exact impedance (Figure S11 (e) and Figure S12 (a), respectively). The DRTs recovered with the re-im CV and kf-CV methods are characterized by a higher uncertainty as evidenced by broader confidence bands (see the grey regions in panels (d) and (f) of Figure S12, respectively). Furthermore, Table S6 displays the values of the quality scores for each method. Similar to the white noise case (Sections 3.1.1.1 and 3.1.1.3), GCV appears to outperform all other methods. Figures S13 and S14 show the averaged recovered impedances and DRTs for each method studied and the noise model in (21b). Consistent with our

findings, we note that GCV and mGCV methods led to satisfactory impedance and DRT recovery, LC and rGCV under-recovered the DRT while re-im CV and kf-CV were more uncertain.

3.1.2 2×ZARC Model

Next, we studied the standard $2\times$ZARC model with overlapping ($\tau_1 = 10^{-1}$ s, $\tau_2 = 10^{-2}$ s), separated ($\tau_1 = 10^{-1}$ s, $\tau_2 = 10^{-4}$ s), and distant ($\tau_1 = 1$ s, $\tau_2 = 10^{-4}$ s) timescales. We proceeded in the same manner as the single ZARC model and started with a single synthetic experiment for the overlapping 2×ZARC model. The recovered impedances and DRTs are displayed in Figure 5 and Figures S15-S16. The DRT peaks were well identified for all the methods and the impedance was closely recovered. The boxplots of the obtained λ and $\mathrm{SE}_{\mathrm{norm},\gamma}$ are shown in panels (c) and (d) of Figure 3, respectively. The marginal distribution and correlation plots of the selected λ against λ_{opt} are displayed in Figure S17. Consistent with the conclusions for the single ZARC model, we find that the GCV method outperforms all other parameter regularization methods (see the lower values of all the quality scores in Table S7).

Next, we studied the separated 2×ZARC model. The DRTs and impedances were well recovered as shown in Figure 6 and Figures S18-S19. Panel (a) of Figures S20 and S21 show the boxplot of λ values obtained and $\mathrm{SE}_{\mathrm{norm},\gamma}$ values, respectively, while Table S8 depicts the values for the quality scores. We note that the LC method slightly under-recovered the DRT (Figure S18 (f)). Unsurprisingly, for the distant $2\times$ZARC model with $R_{\mathrm{ct},1} < R_{\mathrm{ct},2}$ and $R_{\mathrm{ct},1} > R_{\mathrm{ct},2}$ whose parameter values are reported in Table S3, the LC method under-recovered the DRT, and re-im CV and kf-CV recovered the DRT with significant uncertainty, see Figures S22-S25 and Table S9 for $R_{\mathrm{ct},1} > R_{\mathrm{ct},2}$. We further studied the influence of σ_n^{exp} for the overlapping, separated, and distant ($R_{\mathrm{ct},1} > R_{\mathrm{ct},2}$) 2×ZARC models, and we observed that the selected λ values for all the

methods were closer to the optimal value λ_{opt}, but slightly affected by higher σ_n^{exp} (Tables S7-S9). The GCV and mGCV methods consistently outperformed all the parameter regularization methods, even when the EIS data was corrupted with noise (21) in Section 2.2 (Figures S26-S37 and Tables S10-S12).

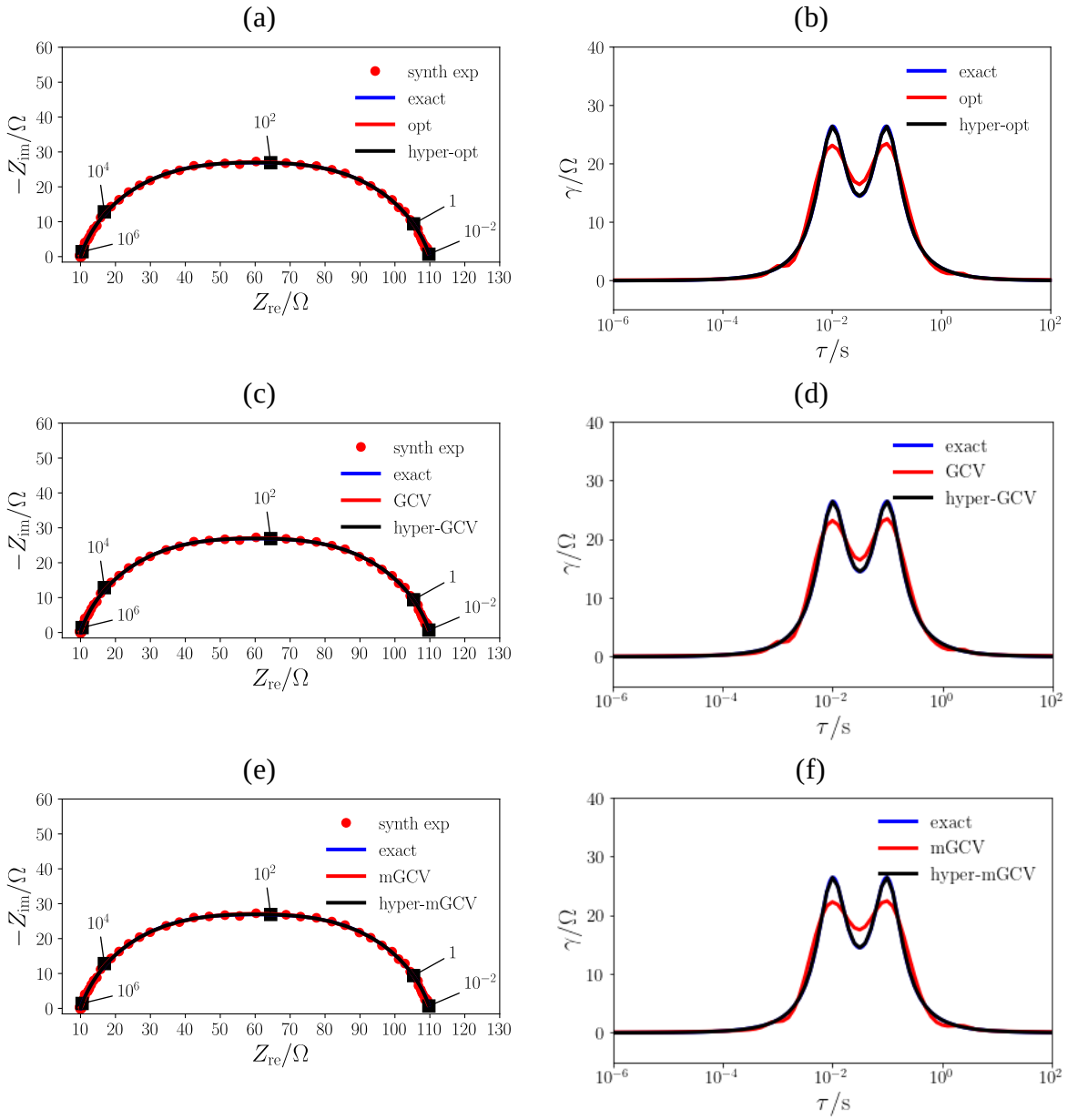

Figure 5. For the overlapping 2×ZARC model ($\sigma_n^{\mathrm{exp}} = 0.2\ \Omega$), exact, experimental, and recovered impedances based on (a) optimal and hyper-optimal, (c) GCV and hyper-GCV, and (e) mGCV and hyper-mGCV methods are shown. Exact and recovered DRTs are shown in panels (b), (d), and (f).

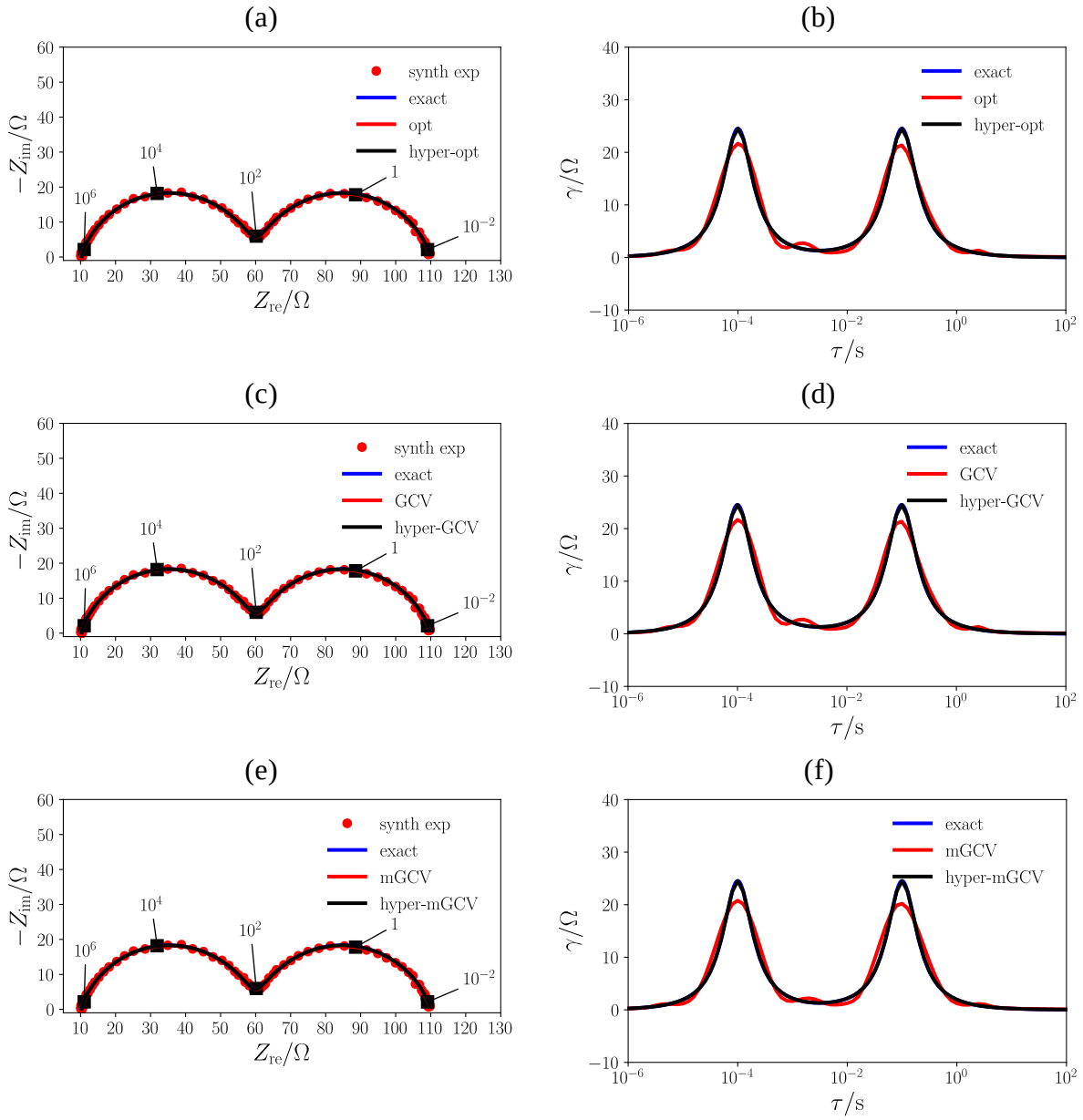

Figure 6. For the separated 2×ZARC model ($\sigma_n^{\mathrm{exp}} = 0.2\,\Omega$), exact, experimental, and recovered impedances based on (a) optimal and hyper-optimal, (c) GCV and hyper-GCV, and (e) mGCV and hyper-mGCV methods are shown. Exact and recovered DRTs are shown in panels (b), (d), and (f).

3.1.3 Piecewise Constant and Gerischer Models

To investigate whether the proposed methods can capture discontinuities in the DRT, the PWC and Gerischer models were also studied [30,31,50]. Figure 7 and Figures S38-S39 show the averaged recovered Nyquist plots and DRTs for the PWC. Consistent with the single and 2×ZARC models, the LC method slightly under-recovered the exact DRT while the re-im CV and kf-CV methods led to the recovered DRTs with larger uncertainty (see Figure 3, Figure 7, and Figures S38-39). For the Gerischer model, the same conclusion can be reached as for the PWC model (Figure 8 and Figures S40-S41). Due to their proximity to the optimal method and their lower uncertainty, the GCV and mGCV methods appeared to outperform the other methods, including when the error level increased and when the noise was modeled according to (21) (Figures S42-S49, and Tables S13-S16).

So far, we have used a fixed number N of collocation points ($N = 81$ log timescales). Therefore, we also investigated the influence of the number N on the accuracy of the DRT recovery. Specifically, we studied the cases $N = 41, 61, 101,$ and 121 log timescales, and found that the DRT recovery using GCV and mGCV were the most accurate as N increased (see Figure S50-S57 and Table S17).

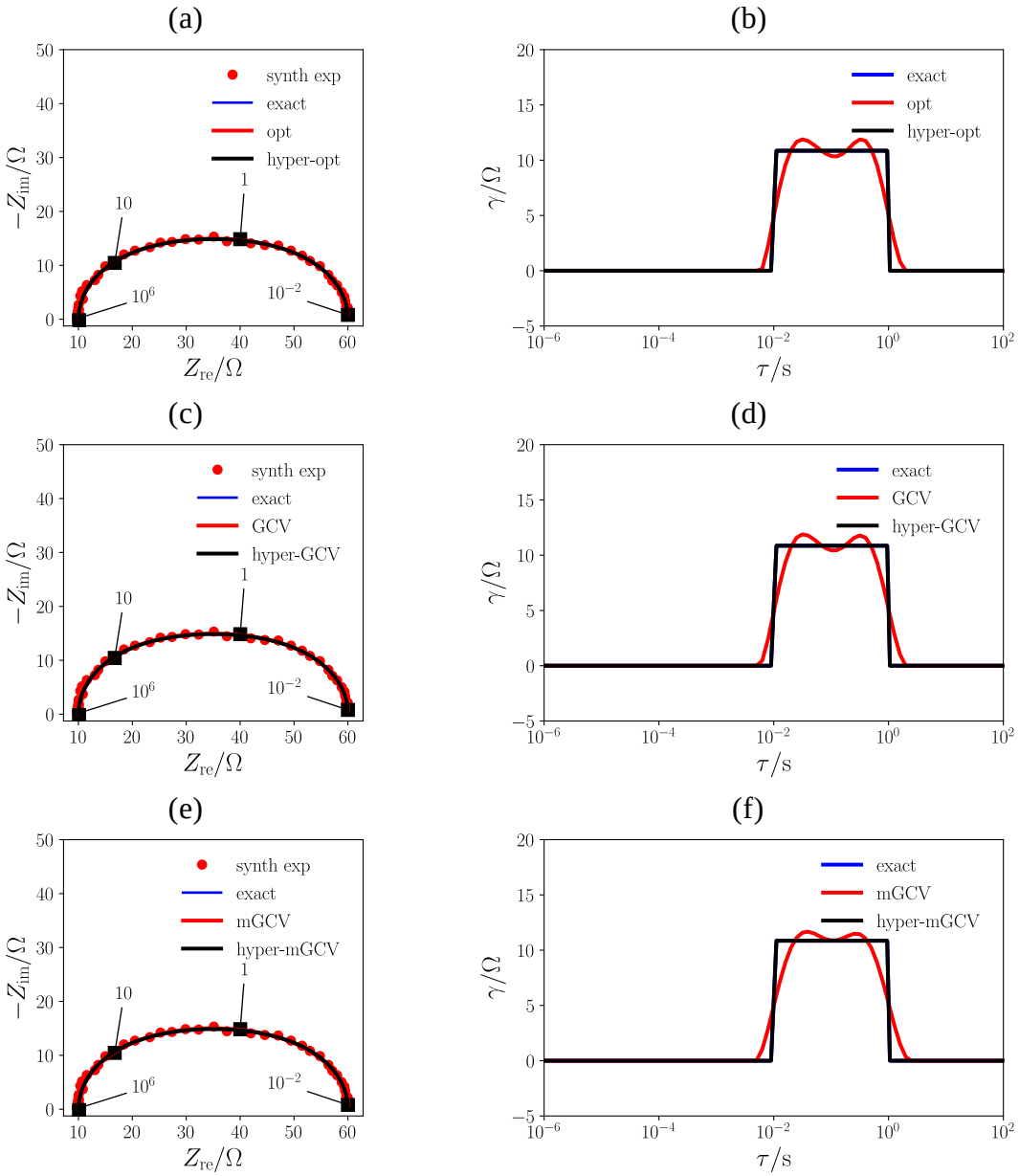

Figure 7. For the PWC model ($\sigma_n^{\mathrm{exp}} = 0.2\,\Omega$), exact, experimental, and recovered impedances based on (a) optimal and hyper-optimal, (c) GCV and hyper-GCV, and (e) mGCV and hyper-mGCV methods are shown. Exact and recovered DRTs are shown in panels (b), (d), and (f).

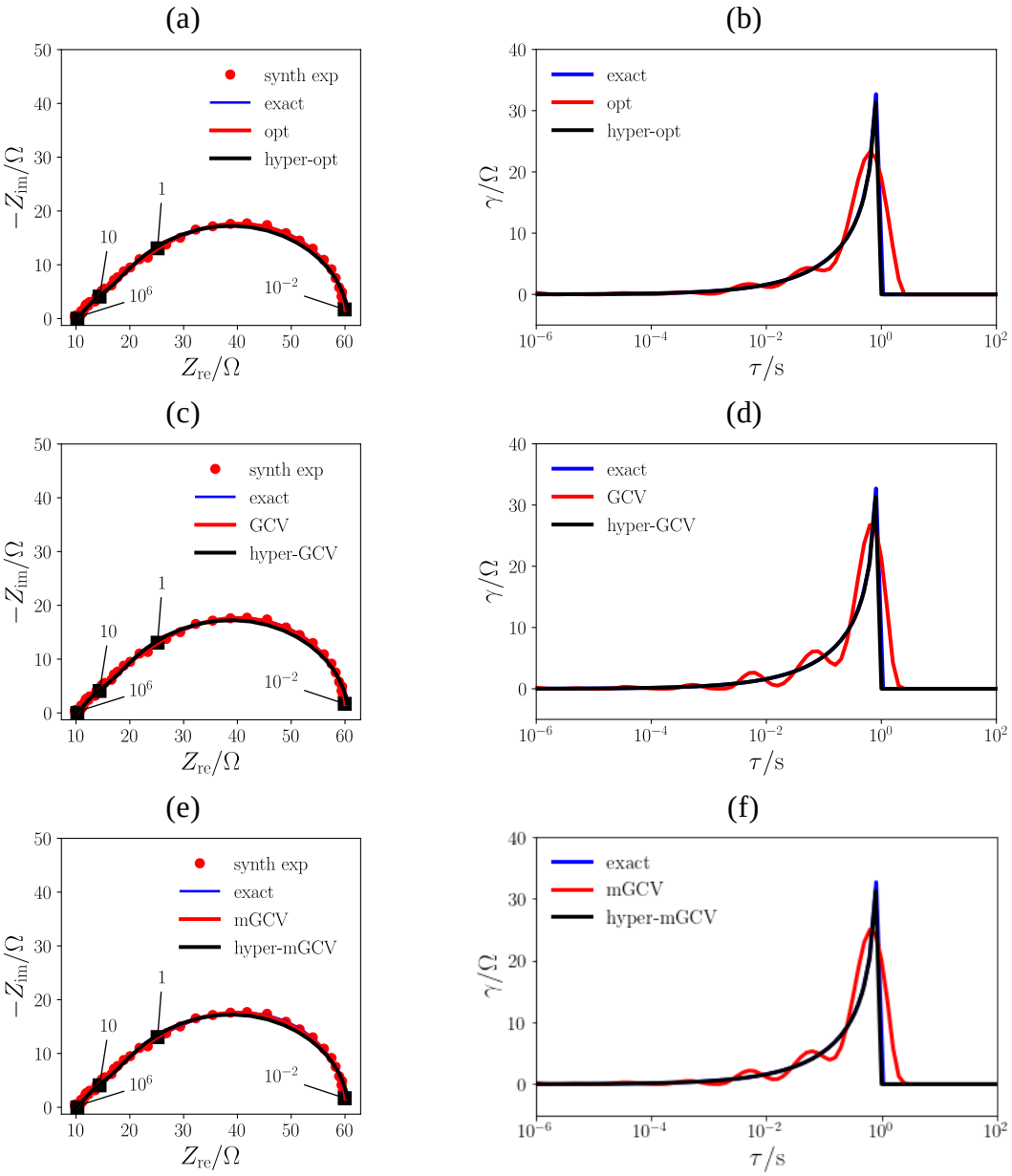

Figure 8. For the Gerischer model ($\sigma_n^{\mathrm{exp}} = 0.2\ \Omega$), exact, experimental, and recovered impedances based on (a) optimal and hyper-optimal, (c) GCV and hyper-GCV, and (e) mGCV and hyper-mGCV methods are shown. Exact and recovered DRTs are shown in panels (b), (d), and (f).

3.1.4 "**Hook**" **Model**

We tested whether the proposed methods are also applicable when the impedance is characterized by high-frequency "inductive" loops [51]. The left and right panel of Figure 9 and Figures S58-S59 show the averaged recovered impedances and DRTs for each method, respectively. Similar to the single ZARC, 2×ZARC, PWC, and Gerischer models, we observed that the LC method led to over-smooth DRTs and mismatched impedances (Figure S58 (f)). Conversely, the re-im CV and kf-CV methods are characterized by a larger uncertainty, leading to more significant confidence bands (panels (d) and (f) of Figure S59). Due to their proximity to the optimal method and narrow confidence bands, we conclude that the GCV and mGCV methods outperform all the other methods under study (Table S18), even when the experimental noise level increases and when the noise is modeled with error models (21) in Section 2.2, see Figures S60-S63 and Tables S18-S19.

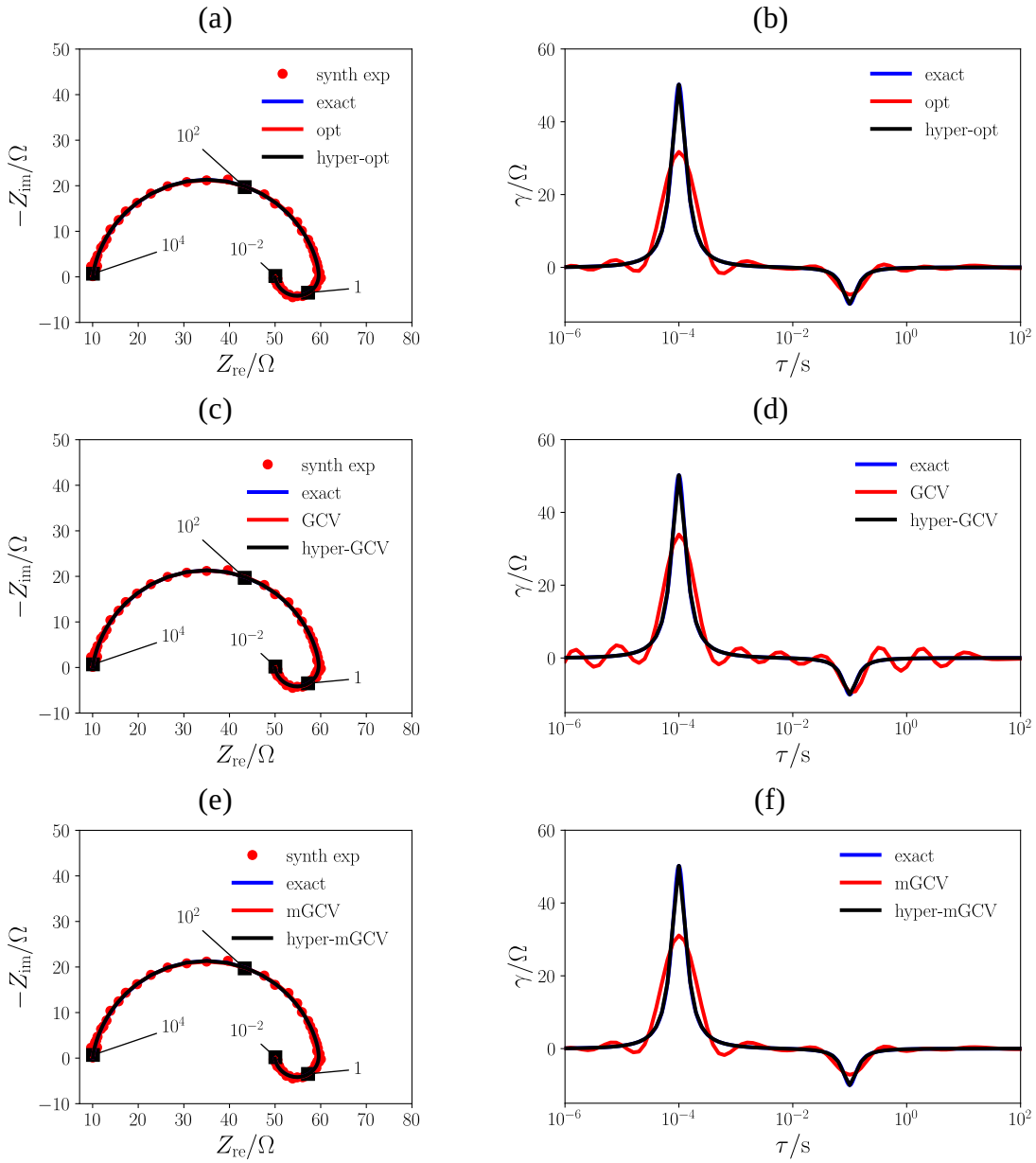

Figure 9. For the "hook" model ($\sigma_n^{\mathrm{exp}} = 0.2\,\Omega$), exact, experimental, and recovered impedances based on (a) optimal and hyper-optimal, (c) GCV and hyper-GCV, and (e) mGCV and hyper-mGCV methods are shown. Exact and recovered DRTs are shown in panels (b), (d), and (f).

3.1.5 Hyper-λ

Due to the closeness to the optimal λ_{opt} and least uncertainty, we identified the GCV and mGCV methods as the two most accurate approaches amongst all methods. Therefore, the nominal regularization level, λ_0, in (11), which is analogous to λ in RR, was selected, leveraging the optimal, GCV, and mGCV scores. To compare these three methods against the corresponding hyper-λ method, we generated a synthetic experiment (N = M = 81) with $\sigma_n^{\text{exp}} = 0.2\ \Omega$ for the single ZARC, each 2×ZARC, the PWC, and the Gerischer models. Then, we recovered the DRTs and impedances, leveraging the iterative algorithm described elsewhere [31].

3.1.5.1 Single ZARC Model

Figure 2 shows the averaged recovered impedances and DRTs obtained using hyper method with $\lambda_{0,\text{opt}}$ and the $\lambda = \lambda_0$ from the GCV and mGCV methods. The DRTs peaks were better identified by hyper-λ method relative to RR with lower normalized impedance mean square errors (*i.e.*, $\text{MSE}_{\text{norm},Z_{\text{exp}}}$, $\text{MSE}_{\text{norm},Z_{\text{exact}}}$, and $\text{MSE}_{\gamma_{\text{norm,exact}}}$, see Tables S20 and S21).

3.1.5.2 Overlapping, Separated, and Distant 2×ZARC Models

Figure 5, Figure 6, and Figure S65 show the recovered impedances and DRTs for the overlapping, separated, and distant 2×ZARC models, respectively. Consistent with Section 3.1.5.1, the hyper-λ methods outperformed the classical optimal, GCV, and mGCV methods by closely identifying the DRT peaks (Figure S64), which resulted in lower normalized impedance mean square errors as shown in Tables S20 and S21.

3.1.5.3 Discontinuous DRTs

Usually, RR is not able to adequately capture the position of discontinuities, even when the optimal λ_{opt} is used. Interestingly, the hierarchical Bayesian regularization method, which allows a

variation of λ with respect to the log timescale $\log \tau$, has proven to satisfactorily capture the DRT discontinuities [30,31]. Therefore, we extended our analysis to the PWC and Gerischer models. The left and right panels of Figure 7 shows the recovered impedances and DRTs for the PWC model using the hyper-opt, hyper-GCV, and hyper-mGCV methods. For the hyper-opt, hyper-GCV, and hyper-mGCV methods, the recovered impedances and DRTs closely matched the corresponding exact, and the positions of the discontinuities were excellently captured compared to the optimal, GCV, and mGCV methods (see panels (b), (d), and (f) of Figure 7, respectively). The same conclusions can be drawn for the Gerischer model (panels (b), (d), and (f) of Figure 8). Additionally, Tables S22 and S23 gather the computed values of the impedance errors $\mathrm{MSE}_{\mathrm{norm},Z_{\mathrm{exp}}}$, $\mathrm{MSE}_{\mathrm{norm},Z_{\mathrm{exact}}}$, and $\mathrm{MSE}_{\gamma_{\mathrm{norm,exact}}}$ for the opt-, GCV-, and mGCV-based hyper-λ methods, including when the number of collocation points increases. We noticed that both scores were lower for the hyper-λ methods, *i.e.*, these methods led to more precise impedance recoveries of the Gerischer and PWC models compared to RR.

3.1.5.4 DRTs with the "Inductive" Loops

We continued our analysis with the "hook" model. Figure 9 displays the recovered impedances and DRTs. Consistent with the single ZARC, each 2×ZARC, the PWC, and the Gerischer models, the hyper-λ methods captured both the peak and the ring of the "hook" model excellently compared to the corresponding optimal, GCV, and mGCV methods. The "hook" impedance was also closely recovered, see the values of $\mathrm{MSE}_{\mathrm{norm},Z_{\mathrm{exp}}}$, $\mathrm{MSE}_{\mathrm{norm},Z_{\mathrm{exact}}}$, and $\mathrm{MSE}_{\gamma_{\mathrm{norm,exact}}}$ in Table S22.

3.2 Real Experiments

In Section 3.1, GCV and mGCV were identified as the best parameter regularization scores amongst the scores studied. In this section, the RR and hyper-RR are analyzed using real EIS data from three batteries and one fuel cell.

3.2.1 Lithium-ion Batteries

3.2.1.1 Composite Polymer Electrolyte

We first studied the EIS spectrum from a battery with a composite polymer electrolyte, a Li-metal anode, and a $LiFePO_4$ cathode [52]. The EIS frequencies were taken between 1 Hz and 7 MHz with five points per decade, and the ECM parameters are presented in Table S24. Each row of Figure 10 show the impedance (left panel) and DRT (right panel) recovered using the optimal and hyper-opt, GCV and hyper-GCV, and mGCV and hyper-GCV methods. We observed that the hyper-λ approaches recovered the DRT more accurately compared to the corresponding parameter regularization method (panels (b), (d), and (f) of Figure 10 and Table S25 for the values of $\mathrm{MSE}_{\mathrm{norm},Z_{\mathrm{exp}}}$, $\mathrm{MSE}_{\mathrm{norm},Z_{\mathrm{ECM}}}$, and $\mathrm{MSE}_{\gamma_{\mathrm{norm,ECM}}}$[7]).

[7] It is worth stressing that, for real EIS experiments, the exact DRT and impedance are replaced by the ECM-fitted DRT and impedance, respectively. Moreover, no exact value can be given for these scores since the ECM is not unique.

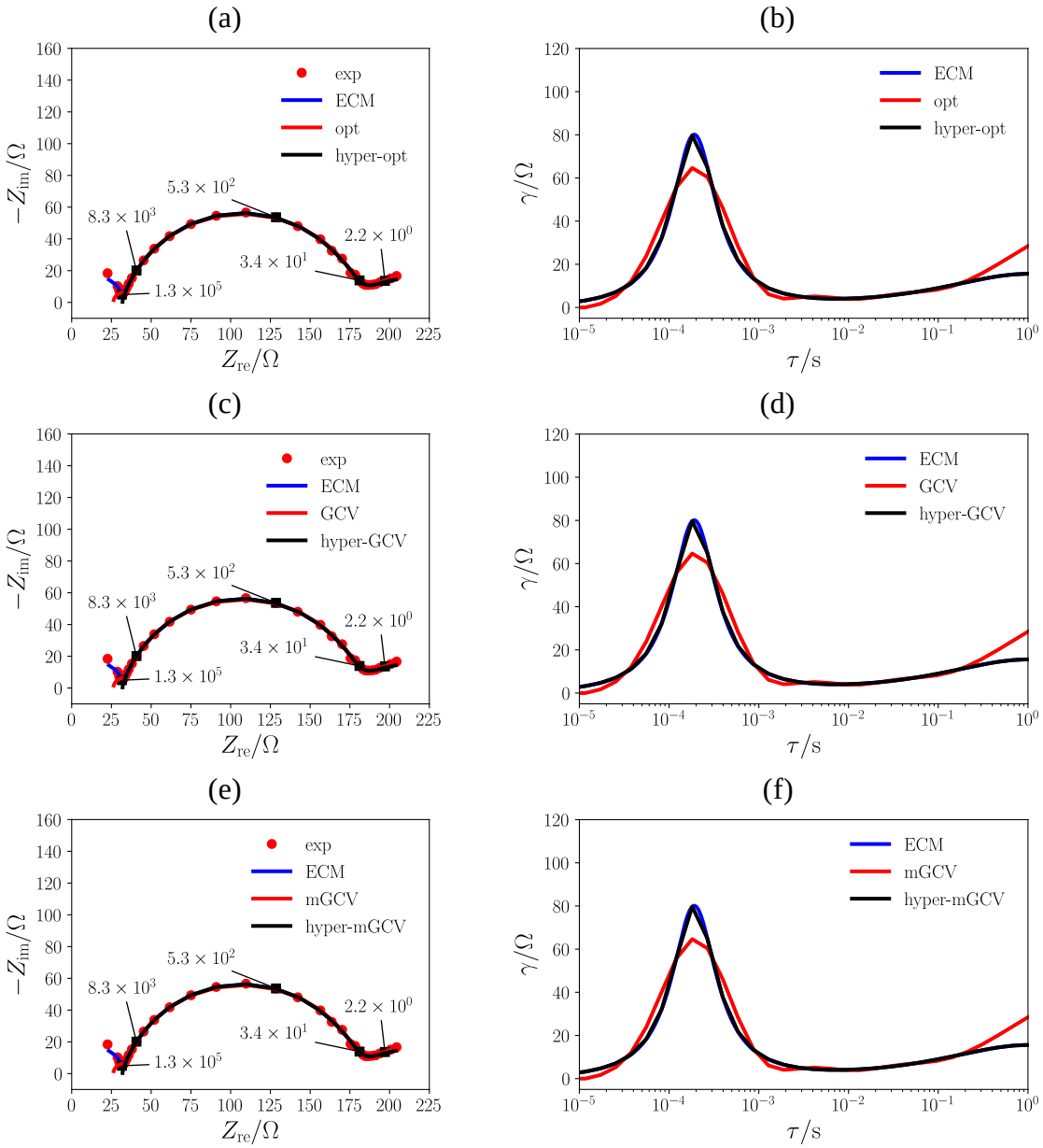

Figure 10. For the battery with a composite polymer electrolyte, ECM-fitted, experimental, and recovered impedances based on the (a) optimal and hyper-optimal, (c) GCV and hyper-GCV, and (e) mGCV and hyper-mGCV methods are shown. ECM-fitted recovered DRTs are shown in panels (b), (d), and (f).

3.2.1.2 Solid-like Dual-Salt Polymer Electrolyte

We investigated EIS data gathered from a battery with the same electrode as the battery studied in Section 3.2.1.1, but with a solid-like dual-salt polymer electrolyte [53]. The results of the DRT and impedance recoveries are displayed in Figure 11 and Table S25 and we found that the hyper-λ methods exceled at recovering the DRT and impedance of this battery.

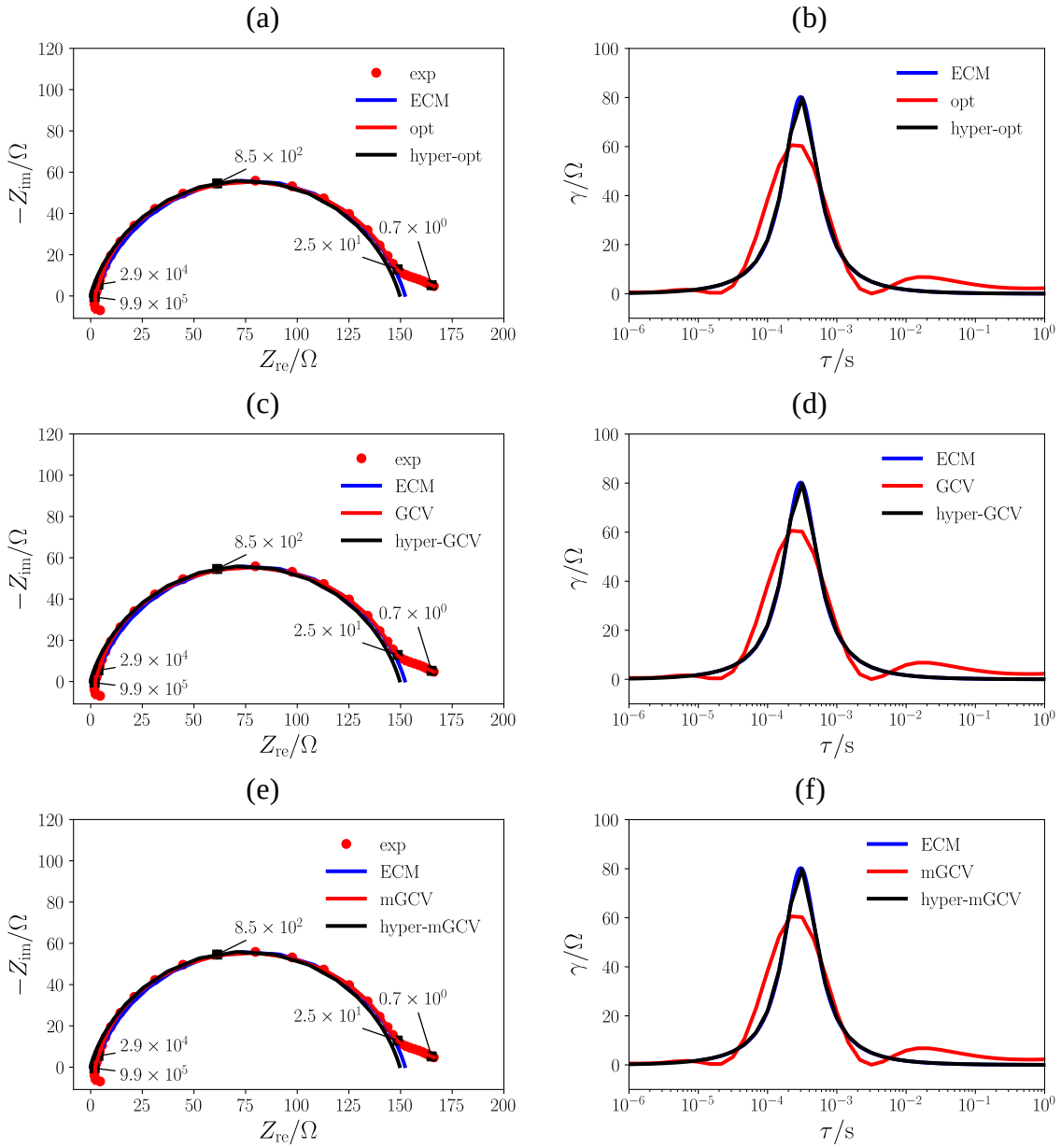

Figure 11. For the DSPE battery, experimental impedance, ECM-fitted impedance, and recovered impedances based on the (a) optimal and hyper-opt, (c) GCV and hyper-GCV, and (e) mGCV and hyper-mGCV methods are shown. ECM-fitted and recovered DRTs are shown in panels (b), (d), and (f).

3.2.1.3 Commercial Li-ion Battery

Next, we investigated the EIS spectrum collected from a Li-ion battery with frequencies in the range from 5 mHz to 600 Hz [18,33] The regressed ECM parameters are reported in Table S24. The recovered impedances and DRTs are displayed in Figure S65. The DRT peak of the estimated DRTs mismatched the peak of the DRT obtained with the ECM, but the impedances were closely recovered. These findings are validated with the values of the quality scores presented in Table S25.

3.2.2 Symmetric Protonic Ceramic Fuel Cell

Lastly, we analyzed data recovered from a symmetric cell with $Sr_{0.9}Ce_{0.1}Fe_{0.8}Ni_{0.2}O_{3-\delta}$ as the electrode material and Ni-$BaZr_{0.1}Ce_{0.7}Y_{0.1}Yb_{0.1}O_{3-\delta}$ as the electrolyte at 500℃ in an atmosphere of 93% Air-6% H_2O [54]. The probed frequencies ranged from 0.01 Hz to 200 kHz with five points per decade. The ECM parameters are reported in Table S24. The DRT and impedances recovered with each method are shown in Figure 12. The results confirm that the hyper-λ methods outperformed the other methods, which was further validated by the low values of $\mathrm{MSE}_{\mathrm{norm},Z_{\mathrm{exp}}}$, $\mathrm{MSE}_{\mathrm{norm},Z_{\mathrm{ECM}}}$, and $\mathrm{MSE}_{\gamma_{\mathrm{norm,ECM}}}$ for each hyper-λ method (Table S25).

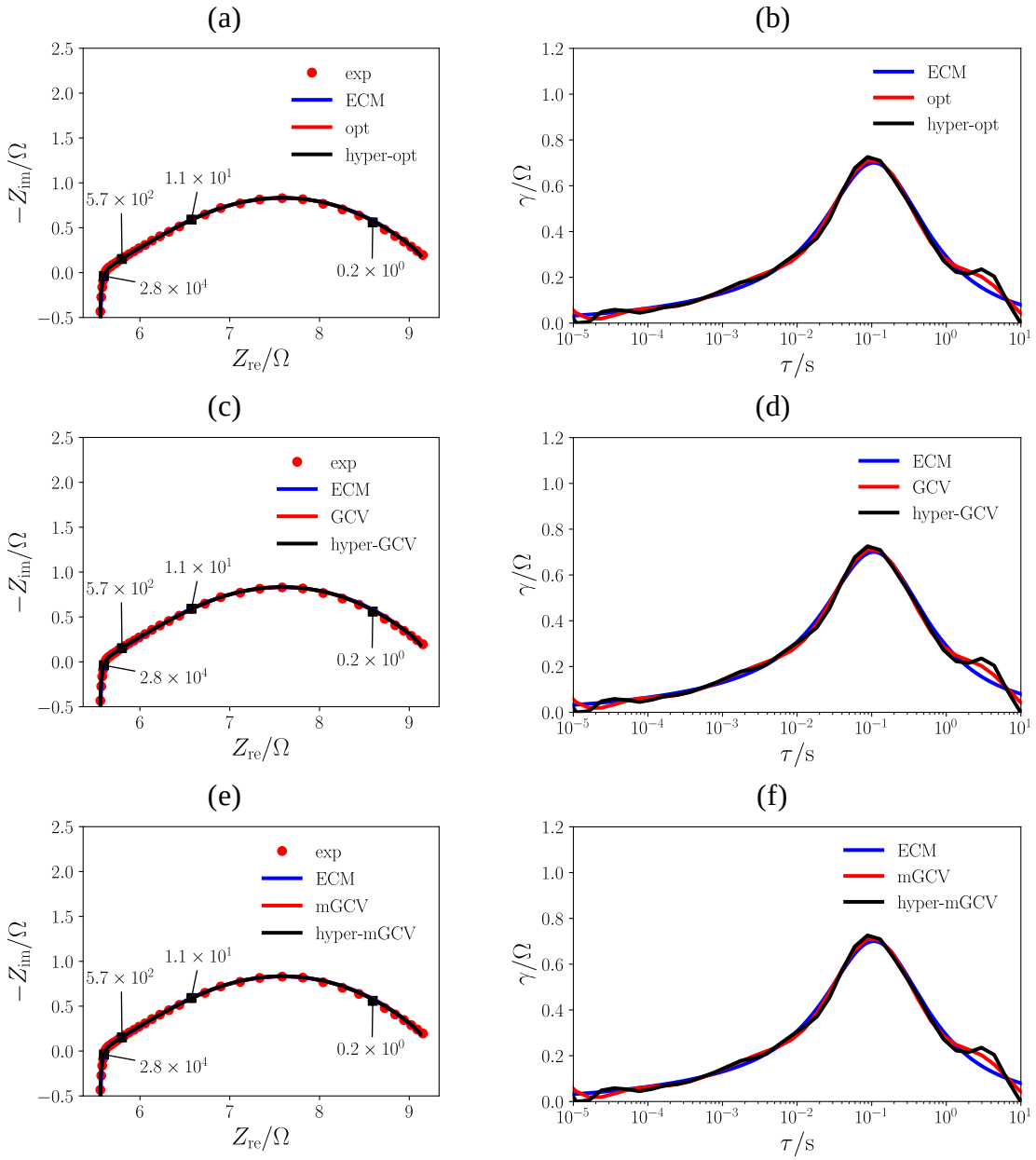

Figure 12. For the symmetric protonic ceramic fuel cell, ECM-fitted, experimental, and recovered impedances based on the (a) optimal and hyper-optimal, (c) GCV and hyper-GCV, and (e) mGCV and hyper-mGCV methods are shown. ECM-fitted and recovered DRTs are shown in panels (b), (d), and (f).

4 Remarks and Future Work

This article provides a thorough investigation of various methods for the selection of the regularization parameter for DRT deconvolution. Despite its broad scope, several opportunities for future extensions can be outlined. First, piecewise linear functions were used to discretize the DRT impedance in (3), but other discretizations (*e.g.*, radial basis functions and neural networks) should also be studied as they are widely used [34]. Second, other hyperparameters aside from λ, namely the parameter β of the hyperprior distribution, the number N of collocation points, the derivative order q of the differentiation matrix $\boldsymbol{L}$ in (2), the partitioning parameter k of the kf-CV, and the minimum $\tau_{\min}$ and maximum $\tau_{\max}$ timescales, could be "optimally" selected. Third, other methods could be studied, including strong robust CV [55], generalized maximum likelihood [38], randomized generalized approximate CV [56], and Mallow C_P [57].

5 Conclusions

Amongst all methods implemented to deconvolve the DRT, RR has been widely applied, but its accuracy still depends upon a regularization parameter that can significantly affect the quality of the DRT and impedance recoveries. In this work, we studied six scores for parameter regularization selection, including five cross-validation scores and the L-curve. Using an array of synthetic experiments, we showed that the GCV and mGCV scores outperformed the other scores studied. Additionally, we extended the previously developed hyper-Bayesian approach by leveraging the GCV and mGCV scores. Then, we showed with various artificial and real EIS spectra that hyperparametric selection recovers DRTs and impedances more precisely than RR. The implementation of the code used to generate these results is provided in pyDRTtools, allowing other researchers to follow up on this work.

Code Availability

Relevant code is available at https://github.com/ciuccilab/pyDRTtools.

Author Credit Statement

Adeleke Maradesa: Software Extension, Software Validation, Data Curation, Formal Analysis, Investigation, Methodology, Simulation, Theory Development, Writing – Original Draft, Writing – Review & Editing. Baptiste Py: Software Extension, Software Validation, Theory Development, Investigation, Writing – Original Draft, Writing – Review & Editing. Ting Hei Wan: Software Extension, Software Validation, Theory Development, Writing, Review & Editing. Mohammed B. Effat: Software Extension, Software Validation, Review & Editing. Francesco Ciucci: Software Creation, Software Development, Software Testing, Conceptualization, Methodology, Theory Development, Investigation, Resources, Editing, Complete Rewriting, Extensive Quality Control and Entropy Mitigation, Funding Acquisition, Project Administration.

Declaration of Competing Interest

None.

Acknowledgments

The authors gratefully acknowledge the Research Grant Council of Hong Kong for support through the projects 16206019 and 16201820. This wok was supported in part by the Project of Hetao Shenzen-Hong-Kong Science and Technology Innovation Corporation Zone (HZQB-KCZYB-2020083). The authors would also like to thank HKUST Fok Ying Tung Research Institute and National Supercomputing Center in Guangzhou Nansha sub-center for providing high-

performance computational resources. Lastly, A. Maradesa and B. Py thank the Hong Kong PhD. Fellowship Scheme for its financial support.

List of Symbols

Greek letters

$\boldsymbol{\gamma}$	Vector of the discretized DRT
$\gamma(\log\tau)$	Distribution of relaxation times
λ	Regularization parameter (λ_{opt} or λ_{CV})
λ_{hyper}	Hyper-λ optimal regularization parameter
σ_n^{exp}	Level of experimental noise for the synthetic experiments
τ	Relaxation time

Latin letters

$\boldsymbol{A}_{\mathrm{re}}$	Discretization matrix for the real part of the impedance
$\boldsymbol{A}_{\mathrm{im}}$	Discretization matrix for the imaginary part of the impedance
$\boldsymbol{L}$	Differentiation matrix
$\boldsymbol{Z}_{\mathrm{DRT}}$	Vector of the regressed impedances
$\boldsymbol{Z}_{\mathrm{exp}}$	Vector of the experimental impedances
$\boldsymbol{x}$	Vector of discretized DRTs for RR
abs_{λ}	Mean absolute distance
$\mathrm{abs}_{\mathrm{norm},\lambda}$	Mean absolute normalized distance

f	Frequency
N	Number of collocation points
M	Number of frequencies
MSE_{λ}	Mean square error of the selected λ
$\mathrm{MSE}_{\mathrm{norm},\gamma}$	Normalized DRT mean square error ($\gamma = \gamma_{\mathrm{opt}}$ or γ_{exact})
$\mathrm{MSE}_{\mathrm{norm},Z}$	Normalized impedance mean square error ($Z = Z_{\mathrm{opt}}$, Z_{exp}, Z_{ECM}, or Z_{exact})
$\mathrm{SE}_{\mathrm{norm},\gamma}$	Normalized DRT square error

List of Abbreviations

CV	Cross-validation
DRT	Distribution of relaxation times
ECM	Equivalent circuit model
EIS	Electrochemical impedance spectroscopy
GCV	Generalized cross-validation
kf-CV	k-fold cross-validation
LC	L-curve
MAP	Maximum a posteriori
mGCV	Modified generalized cross-validation
PWC	Piecewise constant

re-im CV	Real imaginary cross-validation
rGCV	Robust generalized cross-validation
RR	Ridge regression

References

[1] C. Byoung-Yong, P. Su-Moon, Electrochemical impedance spectroscopy, Annual Rev. Anal. Chem. 3 (2010) 29–207.

[2] F.E. Bedoya-Lora, I. Holmes-Gentle, A. Hankin, Electrochemical techniques for photoelectrode characterization, Curent Opinion in Green and Sustainable Chemistry. 29 (2021) 100463.

[3] H. Nara, T. Yokoshima, T. Osaka, Technology of electrochemical impedance spectroscopy for an energy-sustanined society, Current Opinion in Electrochemistry. 20 (2020) 66–77.

[4] I.D. Raistrick, Application of impedance spectroscopy to materials science, Annual Rev. Mater. Sci. 16 (1986) 343–370.

[5] S.B. Rutkove, Electrical impedance myography: Background, current state and future direction, Muscle Nerve. 40 (2009) 936–946.

[6] K. Krukiewicz, Electrochemical impedance spectroscopy as a versatile tool for the characterization of neural tissue: A mini review, Electrochemistry Communications. 116 (2020) 106742.

[7] D.D. Macdonald, Reflections on the history of electrochemical impedance spectroscopy, 51 (2006) 1376–1388.

[8] F. Ciucci, Modeling electrochemical impedance spectroscopy, Current Opinion in Electrochemistry. 13 (2019) 132–139.

[9] D. Klotz, J.P. Schmidt, A. Kromp, A. Weber, E. Ivers-Tiffée, The distribution of relaxation times as beneficial tool for equivalent circuit modeling of fuel cells and batteries, ECS Trans. 41 (2019) 25–33.

[10] A. Maradesa, B. Py, E. Quattrocchi, F. Ciucci, The probabilistic deconvolution of the distribution of relaxation times with finite Gaussian processes, Electrochim. Acta. 413 (2022) 140119.

[11] E. Quattrocchi, T.H. Wan, A. Belotti, D. Kim, S. Pepe, S.V. Kalinin, M. Ahmadi, F. Ciucci, The deep-DRT: A deep neural network approach to deconvolve the distribution of relaxation times from multidimensional electrochemical impedance spectroscopy data, Electrochim. Acta. 392 (2021) 139010.

[12] D. Medvedev, Distribution of relaxation time analysis for solid state electrochemistry, Electrochim. Acta. 360 (2020) 137034.

[13] B.A. Boukamp, A. Rolle, Use of a distribution function of relaxation times (DFRT) in impedance analysis of SOFC electrodes, Solid State Ionics. 314 (2018) 103–111.

[14] N. Schlüter, S. Ernst, U. Schröder, Finding the optimal regularization parameter in distribution of relaxation times analysis, ChemElectroChem. 6 (2019) 6027–6037.

[15] N. Florsch, C. Camerlynck, A. Revil, Direct estimation of the distribution of relaxation times from induced-polarization spectra using a Fourier transform, Near Surface Geophysics. (2012) 517–531.

[16] K. Kobayashi, T.S. Suzuki, Extended distribution of relaxation times analysis for electrochemical impedance spectroscopy, Electrochem. 90 (2022) 017004.

[17] M.A. Danzer, Generalized distribution of relaxation times analysis for the characterization of impedance spectra, Batteries. 5 (2019) 53.

[18] J. Liu, F. Ciucci, The Gaussian process distribution of relaxation times: A machine learning tool for the analysis and prediction of electrochemical impedance spectroscopy data, Electrochim. Acta. 331 (2020) 135316.

[19] J. Weese, A reliable and fast method for the solution of Fredholm integral equations of the first kind based on Tikhonov regularization, Computer Physics Communications. 69 (1992) 99–111.

[20] A.C. Alvarez, G. Hime, D. Marchesin, P.G. Bedrikovetsky, The inverse problem of determining the filtration function and permeability reduction in flow of water with particles in porous media, Transp Porous Med. 70 (2007) 43–62.

[21] J. Kaipio, E. Somersalo, Statistical inverse problems: Discretization, model reduction and inverse crimes, Journal of Computational and Applied Mathematics. 198 (2007) 493–504.

[22] A.N. Tikhonov, A.V. Goncharsky, V.V. Stepanov, A.G. Yagola, Numerical methods for the solution of ill-posed problems, Springer Netherlands, Dordrecht, 1995.

[23] S.V. Pereverzev, S.G. Solodky, V.B. Vasylyk, M. Žic, Regularized collocation in distribution of diffusion times applied to electrochemical impedance spectroscopy, Computational Methods in Applied Mathematics. 20 (2020) 517–530.

[24] S. Hershkovitz, S. Tomer, S. Baltianski, Y. Tsur, ISGP: Impedance spectroscopy analysis using evolutionary programming procedure, ECS Trans. 33 (2019) 67–73.

[25] A.B. Tesler, D.R. Lewin, S. Baltianski, Y. Tsur, Analyzing results of impedance spectroscopy using novel evolutionary programming techniques, J Electroceram. 24 (2010) 245–260.

[26] B.A. Boukamp, Fourier transform distribution function of relaxation times; application and limitations, Electrochim. Acta. 154 (2015) 35–46.

[27] T. Hörlin, Deconvolution and maximum entropy in impedance spectroscopy of noninductive systems, Solid State Ionics. 107 (1998) 241–253.

[28] J. Liu, F. Ciucci, The deep-prior distribution of relaxation times, J. Electrochem. Soc. 167 (2020) 026506.

[29] F. Ciucci, The Gaussian process Hilbert transform (GP-HT): Testing the consistency of electrochemical impedance spectroscopy data, J. Electrochem. Soc. 167 (2020) 126503.

[30] M.B. Effat, F. Ciucci, Bayesian and hierarchical Bayesian based regularization for deconvolving the distribution of relaxation times from electrochemical impedance spectroscopy data, Electrochim. Acta. 247 (2017) 1117–1129.

[31] F. Ciucci, C. Chen, Analysis of electrochemical impedance spectroscopy data using the distribution of relaxation times: A Bayesian and hierarchical Bayesian approach, Electrochim. Acta. 167 (2015) 439–454.

[32] J. Huang, M. Papac, R. O'Hayre, Towards robust autonomous impedance spectroscopy analysis: A calibrated hierarchical Bayesian approach for electrochemical impedance spectroscopy (EIS) inversion, Electrochim. Acta. 367 (2021) 137493.

[33] M. Saccoccio, T.H. Wan, C. Chen, F. Ciucci, Optimal regularization in distribution of relaxation times applied to electrochemical impedance spectroscopy: Ridge and lasso regression methods - a theoretical and experimental study, Electrochim. Acta. 147 (2014) 470–482.

[34] T.H. Wan, M. Saccoccio, C. Chen, F. Ciucci, Influence of the discretization methods on the distribution of relaxation times deconvolution: Implementing radial basis functions with DRTtools, Electrochim. Acta. 184 (2015) 483–499.

[35] M.A. Lukas, F.R. de Hoog, R.S. Anderssen, Efficient algorithms for robust generalized cross-validation spline smoothing, Journal of Computational and Applied Mathematics. 235 (2010) 102–107.

[36] M. Eckert, L. Kolsch, S. Hohmann, Fractional algebraic identification of the distribution of relaxation times of battery cells, in: 2015 54th IEEE Conference on Decision and Control (CDC), IEEE, Osaka, 2015: pp. 2101–2108.

[37] M.A. Lukas, F.R. de Hoog, R.S. Anderssen, Practical use of robust GCV and modified GCV for spline smoothing, Comput Stat. 31 (2016) 269–289.

[38] G. Wahba, A comparison of GCV and GML for choosing the smoothing parameter in the generalized spline smoothing problem, Ann. Statist. 13 (1985) 1378–1402.

[39] S. Effendy, J. Song, M.Z. Bazant, Analysis, design, and generalization of electrochemical impedance spectroscopy (EIS) inversion algorithms, J. Electrochem. Soc. 167 (2020) 106508.

[40] T. Fushiki, Estimation of prediction error by using K-Fold cross-validation, Stat Comput. 21 (2011) 137–146.

[41] P.C. Hansen, D.P. O'Leary, The use of the L-curve in the regularization of discrete ill-posed problems, SIAM J. Sci. Comput. 14 (1993) 1487–1503.

[42] T. Paul, P.W. Chi, P.M. Wu, M.K. Wu, Computation of distribution of relaxation times by Tikhonov regularization for Li ion batteries: usage of L-curve method, Sci Rep. 11 (2021) 12624.

[43] P. Refaeilzadeh, L. Tang, H. Liu, Cross-validation, Springer, New York, NY. (2016).

[44] Y.J. Kim, C. Gu, Smoothing spline Gaussian regression: More scalable computation via efficient approximation, Journal of Royal Statistical Society. 66 (2004) 337–356.

[45] M. Kuhn, K. Johnson, Applied predictive modeling, Springer New York, New York, NY, 2013.

[46] M.P.J Van der Loo, Distribution based outlier detection in univariate data, Statisctics Netherlands. (2010).

[47] A.-K. Hjelm, G. Lindbergh, Experimental and theoretical analysis of $LiMn_2O_4$ cathodes for use in rechargeable lithium batteries by electrochemical impedance spectroscopy (EIS), Electrochim. Acta. 47 (2002) 1747–1759.

[48] P. Su-Moon, Y. Jung-Suk, Electrochemical impedance spectroscopy for better electrochemical measurements, Anal. Chem. 75 (2003) 455A-461A.

[49] A. Lasia, Electrochemical impedance spectroscopy and its applications, Springer New York, New York, NY, 2014.

[50] B.A. Boukamp, Derivation of a distribution function of relaxation times for the (fractal) finite length Warburg., Electrochim. Acta. 252 (2017) 154–163.

[51] D. klotz, Negative capacitance or inductive loop -A general assessment of a common low frequency impedance feature, Electrochemistry Communications. 98 (2019) 58–62.

[52] Z. Dai, J. Yu, J. Liu, R. Liu, Q. Sun, D. Chen, F. Ciucci, Highly conductive and nonflammable composite polymer electrolytes for rechargeable quasi-solid-state Li-metal batteries, Journal of Power Sources. 464 (2020) 228182.

[53] J. Yu, J. Liu, X. Lin, H.M. Law, G. Zhou, S.C.T. Kwok, M.J. Robson, J. Wu, F. Ciucci, A solid-like dual-salt polymer electrolyte for Li-metal batteries capable of stable operation over an extended temperature range, Energy Storage Materials. 37 (2021) 609–618.

[54] Y. Song, J. Liu, Y. Wang, D. Guan, A. Seong, M. Liang, M.J. Robson, X. Xiong, Z. Zhang, G. Kim, Z. Shao, F. Ciucci, Nanocomposites: A new opportunity for developing highly active and durable bifunctional air electrodes for reversible protonic ceramic cells, Adv. Energy Mater. 11 (2021) 2101899.

[55] M.A. Lukas, Strong robust generalized cross-validation for choosing the regularization parameter, Inverse Problems. 24 (2008) 034006.

[56] G. Wahba, Support vector machines, reproducing kernel Hilbert spaces and the randomized generalized approximate cross-validation (GACV), MIT Press. (1999) 69–88.

[57] K.C. Li, Asymptotic Optimality for C_P, C_L, Cross-validation and generalized cross-validation: Discrete Index Set, Ann. Statist. 15 (1987).